UNIVERSIDADE FEDERAL DE ITAJUBÁ - UNIFEI
PROGRAMA DE PÓS-GRADUAÇÃO EM ENGENHARIA ELÉTRICA

A Modified Dijkstra Algorithm to Analyze the Effects of Power Loop Flows Caused by Embedded HVDC Links.

Gabriel Ferreira Alvarenga

March 2025

UNIVERSIDADE FEDERAL DE ITAJUBÁ - UNIFEI
PROGRAMA DE PÓS-GRADUAÇÃO EM ENGENHARIA ELÉTRICA

A Modified Dijkstra Algorithm to Analyze the Effects of Power Loop Flows Caused by Embedded HVDC Links.

Gabriel Ferreira Alvarenga

Dissertation submitted to the Graduate Program in Electrical Engineering of the Federal University of Itajubá (UNIFEI) as part of the requirements for obtaining the title of Doctor in Electrical Engineering, with emphasis in Power Systems.

Supervisors:
Antonio Carlos Zambroni de Souza
Glauco Nery Taranto
Bala Venkatesh

Resumo

A tecnologia de Corrente Contínua de Alta Tensão (HVDC) desempenha um papel crucial na integração de energia renovável e na otimização dos fluxos de potência em redes elétricas modernas. Este estudo desenvolve uma estrutura avançada de otimização para minimizar perdas de potência em sistemas com enlaces HVDC incorporados, abordando também os desafios impostos pelas interações de fluxos em laço. Primeiramente, é proposta uma nova metodologia para identificar e analisar cenários de fluxos em laço, utilizando um algoritmo de Dijkstra modificado para detectar de forma eficiente caminhos críticos em redes malhadas de grande escala. Essa abordagem simplifica a análise para os operadores do sistema, permitindo uma mitigação mais eficaz de circulações indesejadas de potência. Com base nesses achados, o estudo formula um problema de otimização que ajusta dinamicamente as injeções de potência HVDC para minimizar perdas na transmissão, especialmente durante eventos de redistribuição de potência causados por flutuações na geração renovável. A metodologia considera condições do sistema, como variações de carga e reconfigurações da rede de transmissão, garantindo um desempenho robusto em diferentes cenários operacionais. Simulações nos sistemas de teste de 107 barras do Brasil e 57 barras do IEEE validam a eficácia da estrutura proposta, demonstrando reduções significativas nas perdas de potência e maior eficiência da rede. Os resultados fornecem aos operadores do sistema uma ferramenta abrangente para otimizar a operação de enlaces HVDC, mitigar problemas de fluxos em laço e aprimorar a integração segura de energia renovável no sistema elétrico.

Keywords— Sistemas de transmissão de potência, Otimização de HVDC, Análise de fluxos em laço, Algoritmo de Dijkstra modificado, Minimização de perdas de potência

Abstract

High Voltage Direct Current (HVDC) technology plays a crucial role in integrating renewable energy and optimizing power flows in modern electrical grids. This study develops an advanced optimization framework to minimize power losses in systems with embedded HVDC links while also addressing the challenges posed by loop flow interactions. First, a novel method for identifying and analyzing loop flow scenarios is proposed, utilizing a modified Dijkstra algorithm to efficiently detect critical loop paths in large-scale meshed networks. This approach simplifies the analysis for system operators, enabling more effective mitigation of undesired power circulations. Building upon these findings, the study further formulates an optimization problem that dynamically adjusts HVDC power injections to minimize transmission losses, particularly during power redistribution events caused by renewable generation fluctuations. The methodology considers system conditions such as load variations and transmission network reconfigurations, ensuring robust performance under different operating scenarios. Simulations on the Brazilian 107-Bus and IEEE 57-Bus test systems validate the framework's effectiveness, demonstrating significant reductions in power losses and improved grid efficiency. The findings provide system operators with a comprehensive tool for optimizing HVDC operation, mitigating loop flow issues, and enhancing the secure integration of renewable energy into the power system.

Keywords— Power transmission systems, HVDC optimization, Loop flow analysis, Modified Dijkstra algorithm, Power loss minimization

Acknowledgment

The authors express their sincere gratitude for the financial support provided in part by UNIFEI, Toronto Metropolitan University, Mitacs, CAPES, CNPq, FAPEMIG, and INERGE.

Additionally, we extend our heartfelt appreciation to our families, friends, and supervisors for their unwavering support, encouragement, and guidance throughout this journey. Their contributions have been invaluable to the completion of this work.

"Education is the most powerful weapon which you can use to change the world."
— Nelson Mandela

Contents

List of Figures

List of Tables

1 Introduction

1.1 Motivation

The integration of renewable energy sources has transformed modern power systems, introducing new operational challenges, particularly in managing the variability of wind and solar generation. High Voltage Direct Current (HVDC) technology provides an effective solution by enabling long-distance power transmission with enhanced controllability and lower losses compared to traditional AC transmission. However, when embedded within AC networks, HVDC links can also lead to unintended power circulation and suboptimal power flows, potentially increasing overall system losses. Addressing these challenges requires advanced optimization and control strategies to enhance system efficiency and mitigate undesirable power flow effects.

Brazil's interconnected power system provides a relevant case study, featuring four HVDC transmission links that play a crucial role in transferring surplus renewable generation from the Northeast to major load centers in the Southeast. The country's long-term energy expansion plan highlights the importance of HVDC in strengthening transmission capacity and improving grid flexibility [1]. However, integrating HVDC links has also led to operational challenges, including commutation failures and complex interactions between AC and DC networks [2]. Additionally, studies emphasize the necessity of adaptive HVDC control to mitigate unwanted power circulation and excessive losses [3].

A significant example highlighting these challenges is the August 15, 2023 outage, where a series of transmission instabilities, triggered by protection system malfunctions, led to cascading failures and widespread power imbalances. During this event, wind generation dropped sharply from 17,500 MW to 2,500 MW at 8:30 AM, requiring hydroelectric generation to compensate. However, due to the absence of a fast and efficient control system interconnecting different regions, a significant portion of the load was shed, exacerbating the impact of the disturbance. This event underscores the critical need for enhanced power flow control mechanisms

to prevent large-scale disruptions.

Loop flow, a phenomenon where unintended circulating power flows within the transmission network, represents another key challenge in systems with embedded HVDC links. These flows can lead to increased losses and overloading of transmission lines [4]. In Brazil, loop flow scenarios have been observed, requiring effective strategies to identify, manage, and mitigate their adverse effects on grid efficiency [5].

To address these issues, this study proposes an optimization framework designed to minimize transmission losses in AC systems with embedded HVDC links. Unlike conventional approaches that primarily focus on adjusting HVDC setpoints to mitigate loop flow [3], the proposed methodology dynamically optimizes power flows to enhance overall transmission efficiency. By leveraging real-time adjustments to HVDC injections, the framework ensures better power redistribution during operational changes, such as load variations and transmission line reconfigurations.

Furthermore, to support system operators in analyzing loop flow scenarios, this research incorporates a novel application of the modified Dijkstra algorithm. This algorithm efficiently identifies critical loop paths without requiring prior knowledge of network topology, enhancing monitoring and control capabilities. By combining optimization techniques with advanced pathfinding methods from graph theory, the proposed approach contributes to a more efficient power grid, particularly in regions with a high penetration of renewable energy and multiple HVDC interconnections.

In summary, this work presents an integrated methodology that optimizes HVDC operations to minimize losses while also providing tools for effective loop flow analysis. By improving power flow controllability, the proposed framework enhances the efficiency of power systems, supporting the seamless integration of renewable energy sources and ensuring stable grid operation.

1.2 Literature Review and Previous Works

The circulation of power in closed loops within the grid, known as loop flow, presents significant challenges to system efficiency and loss reduction. Various analytical methods have been developed to study this phenomenon, leveraging statistical and dynamic approaches that account for network impedance, voltage fluctuations, and phase angles. In the context of HVDC systems, research has investigated power flow variations to better understand their impact on electrical network behavior.

More recently, graph theory has emerged as a powerful tool for modeling and analyzing power system topologies. Studies have applied graph-theoretical methods to address congestion management and optimal route planning, demonstrating their effectiveness in improving network operation and identifying critical pathways [6, 7]. Additionally, advancements in static loop analysis and power flow tracing have enhanced system efficiency [8,9]. However, conventional approaches often struggle to capture the complex interactions in modern power networks, especially with the increasing presence of HVDC links.

Building on these graph-theoretical applications, recent research has focused on linear topologies and power system optimization [10, 11]. For instance, a graph-theory-based algorithm has been proposed for loop synthesis, congestion analysis, and power loss allocation in AC networks [6]. These methodologies highlight the necessity for advanced dynamic analysis techniques, particularly as HVDC integration influences loop flow characteristics. Studies have explored embedded HVDC control strategies for renewable energy integration [3] and techniques for mitigating power fluctuations [12]. Additionally, optimization approaches have been introduced to improve system operation and minimize transmission losses in AC/DC hybrid networks [13].

HVDC technology's role in power flow optimization and renewable energy integration has received increasing attention. Research on HVDC system complexity has examined topology design and control strategies [14]. The cost-effectiveness of HVDC-based renewable energy in-

tegration has been analyzed, reinforcing HVDC's advantages for long-distance power transfer [15]. Moreover, methodologies have been introduced to minimize losses in embedded HVDC links, particularly by optimizing back-to-back voltage source converters [16]. The challenges associated with loss reduction in hybrid AC/DC systems further underscore the importance of effective power flow management [17].

Several studies have explored strategies to improve power flow control and loss minimization in HVDC-integrated networks, including the Brazilian power system [3]. A multi-objective optimization technique using the salp swarm algorithm has been proposed to address economic and environmental factors in HVDC operations [18]. Additionally, optimization models incorporating VSC (Voltage Source Converter) losses in hybrid AC/DC configurations have been developed to improve power flow solutions [19].

Computationally efficient optimal power flow approaches for hybrid AC/DC grids have also been introduced, utilizing shift factors to enforce VSC power flow constraints [20]. Metaheuristic optimization algorithms have been explored to minimize fuel costs, pollutant emissions, voltage deviations, and active power losses in hybrid AC/DC networks [21]. Furthermore, extended AC optimal power flow models incorporating VSC-MTDC systems have demonstrated that the effectiveness of VSC-MTDC in loss reduction is highly dependent on system configuration [22].

The impact of renewable energy fluctuations on AC/DC grids with VSC-HVDC has also been a focus, leading to optimal power flow models that leverage VSC capabilities to mitigate power fluctuations [23]. Collectively, these studies emphasize the need for advanced optimization frameworks tailored for HVDC-integrated power systems.

Despite these advancements, a gap remains in methodologies that efficiently identify, analyze, and mitigate loop flow in AC/DC networks. To address this, this work extends previous research by introducing a modified Dijkstra algorithm specifically designed for loop flow identification in HVDC-integrated systems. This algorithm integrates sensitivity analysis to dynamically detect critical pathways affected by HVDC injections,

offering a hybrid approach that combines graph-theoretical techniques with the dynamic conditions of the network. By dynamically adapting to load and generation variations, this methodology provides a more precise representation of critical network pathways and improves power flow efficiency.

Given the rapid transformation of the Brazilian electrical grid and the increasing integration of HVDC systems [2, 3], challenges in power loss reduction and power flow management persist. Despite notable advancements in HVDC control and integration, these issues remain critical. By addressing these limitations, this proposed methodology contributes to broader efforts aimed at enhancing the efficiency and reliability of HVDC-integrated power networks.

1.3 Ph.D. Thesis Statement

This Ph.D. Thesis proposes an analytical approach to identifying, analyzing, and optimizing loop flow caused by HVDC links in electrical power systems. The methodology integrates AC and DC systems by employing Dijkstra's algorithm to efficiently detect loop flow paths and assess their impact on system stability. By pinpointing critical branches affected by HVDC-induced loop flows, this approach enhances grid resilience and optimizes power flow distribution.

Building on this identification process, an optimization framework for HVDC control is developed to minimize transmission losses while maintaining system stability. The proposed methodology dynamically adjusts power flow based on operational constraints and is validated through simulations on the IEEE 57-Bus and Brazilian 107-Bus systems. A key focus is the impact of HVDC placement and generation redistribution on loss minimization, particularly under varying topological and renewable energy conditions.

1.4 Contributions

This study presents an advanced methodology for optimizing power flow and reducing transmission losses in electrical grids with embedded HVDC links. The main contributions of this work are as follows:

- **Loop Flow Analysis and Key Path Identification:** Develops a tool for identifying critical pathways in the AC system affected by HVDC-induced loop flows, pinpointing the most sensitive branches and their impact on system stability.
- **Optimization of System Losses:** Introduces an optimization framework that minimizes total transmission losses by dynamically adjusting HVDC power injections, considering variations in network topology and load conditions.
- **Impact Assessment of Topological Changes:** Evaluates the effects of transmission line openings and network reconfigurations, demonstrating the ability of HVDC control to mitigate negative impacts and enhance system efficiency.
- **Enhanced Decision Support for System Operators:** Provides a practical tool to assist system operators in managing loop flow issues, improving operational planning, and ensuring grid reliability.

By integrating sensitivity analysis with a modified Dijkstra algorithm, this methodology offers a novel and effective approach to loop flow management in HVDC-integrated power systems. The proposed framework enhances grid resilience, optimizes power flow distribution, and provides valuable insights for future research and practical applications in energy transmission networks.

1.5 Ph.D. Thesis Structure

This Ph.D. Thesis is organized into six main chapters, each addressing different aspects of loop flow analysis and optimization in HVDC-integrated power systems.

Chapter 1 introduces HVDC technology in the Brazilian electrical system, outlining the challenges related to loop flow and the research objectives.

Chapter 2 explores the relationship between HVDC systems and the Brazilian power grid, emphasizing operational challenges and the critical role of HVDC in renewable energy integration.

Chapter 3 details the methodology for identifying and analyzing loop flows through a modified Dijkstra algorithm, focusing on identifying critical paths and evaluating their impact on system stability.

Chapter 4 examines the effects of HVDC losses on loop flow, featuring case studies to illustrate the phenomenon within various test systems, including the impact on the IEEE 57-Bus and Brazilian 107-Bus systems.

Chapter 5 discusses the development of the optimization framework aimed at minimizing transmission losses and managing HVDC-induced loop flows, thereby enhancing overall grid efficiency.

Chapter 6 summarizes the key findings of the research, discusses its limitations, and presents recommendations for future studies in the field of power flow management and HVDC integration.

2 Integration of HVDC Technology in the Brazilian Electrical System

This chapter delves into the intricate relationship between HVDC systems and the Brazilian electrical system, with a particular focus on the transmission network's current state and its planned expansion. It begins by outlining the fundamental principles of HVDC technology and the various modeling techniques employed to simulate its behavior within power systems. Subsequently, the chapter provides an overview of the unique characteristics of the Brazilian electrical system, highlighting its transmission network's structure, operational challenges, and existing infrastructure. The discussion then transitions to the critical role of HVDC transmission in facilitating long-distance power transfer, enhancing grid stability, and integrating renewable energy sources.

2.1 Brazilian Interconnected System

The Brazilian electric power system consists of four interconnected subsystems: South, Southeast/Midwest, Northeast, and North, as illustrated in Fig. 1. Each region has distinct characteristics in terms of power generation and load demand [24].

Brazil's HVDC network includes key transmission links [1]:

- Xingu (Pará) to Estreito (Minas Gerais): 4000 MW, 800 kV, 2300 km.
- Anapu (Pará) to Paracambi (Rio de Janeiro): 4000 MW, 2539 km.
- Porto Velho (Rondônia) to Araraquara 2 (São Paulo): 7100 MW, 2375 km.
- Itaipu to Ibiuna (São Paulo): Two 600 kV bipoles, each 3150 MW.

The Southeast/Midwest region, Brazil's largest electricity consumer, primarily relies on hydroelectric and thermoelectric generation, driven by industrial activity and dense urban centers. The South follows a similar energy mix, while the Northeast has significantly expanded wind and

Figure 1: Brazilian electric power system, 2027 horizon. Adapted from [33].

solar power to meet growing demand and seasonal rainfall variability. In contrast, the North, rich in hydroelectric resources, serves as a major electricity exporter to other regions, with HVDC links playing a crucial role in long-distance transmission. Figure 2 highlights these regional differences, showcasing the Northeast's high wind generation capacity, the North's role as a power exporter, and the Southeast/Midwest's status as the heaviest load center in the Brazilian electrical system.

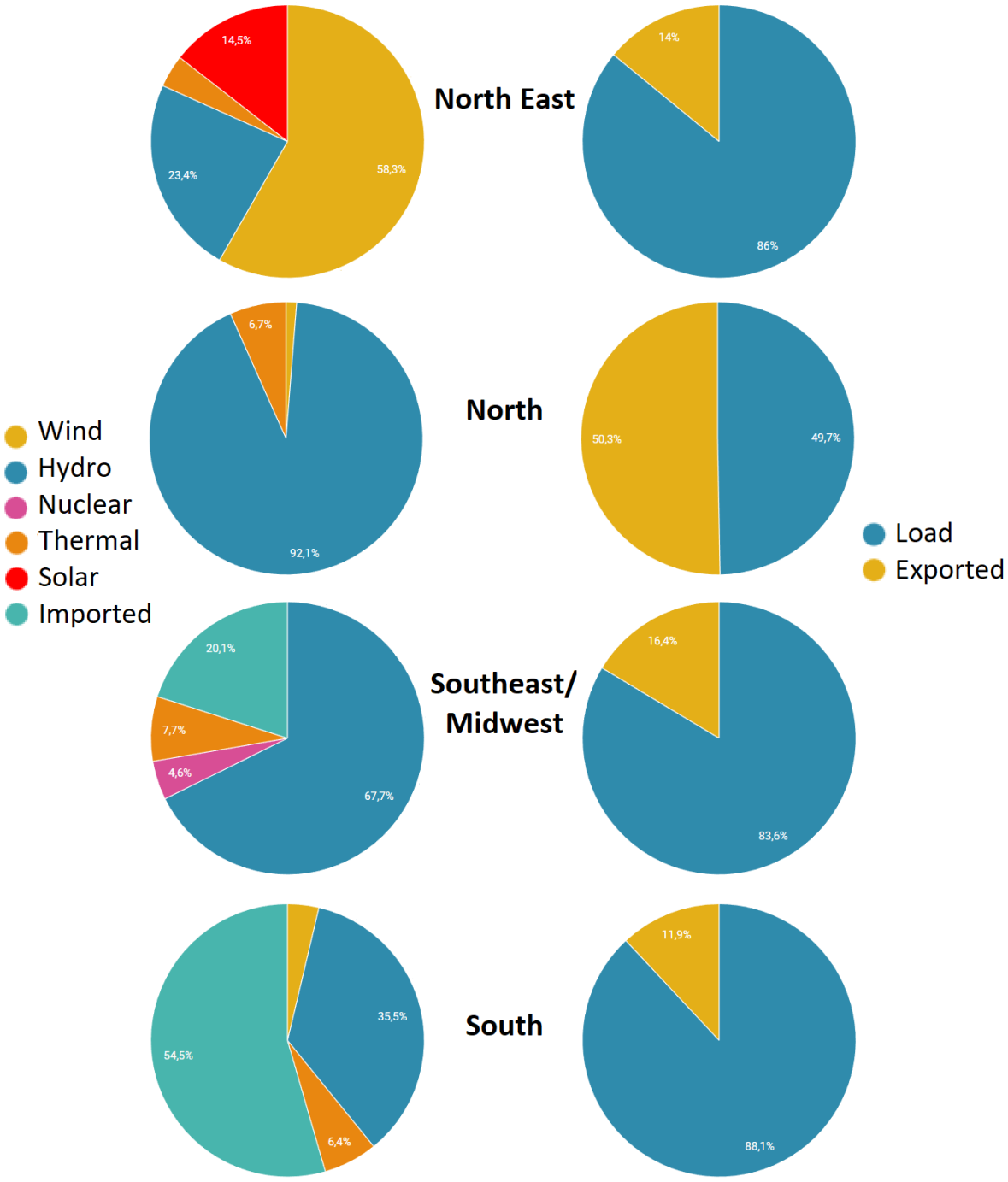

Figure 2: Load and generation rates of the Brazilian electric power system. Adapted from [33].

2.2 Occurrence of Loop Flow in the Brazilian Electrical System

Loop flow, a consequence of transmission congestion, leads to inefficiencies such as load shedding and mismanagement of resources. A reduction in Northeast wind generation induces loop flow propagating southward through HVDC lines and returning via AC lines. A planned 4 GW embedded HVDC system will connect Graça Aranha (Northeast) to Silvânia (Southeast) within five years.

A study by [25] analyzed loop flow using actual measurements. A drop in Northeast wind generation at 8:30 a.m. reversed AC transmission flow between the Northeast and Southeast by 11:00 a.m., with HVDC operation inducing loop flow until 12:30 p.m. (Fig. 3). This phenomenon is particularly relevant when considering past events of large-scale transmission instability in Brazil, such as the loop flow event in 2018.

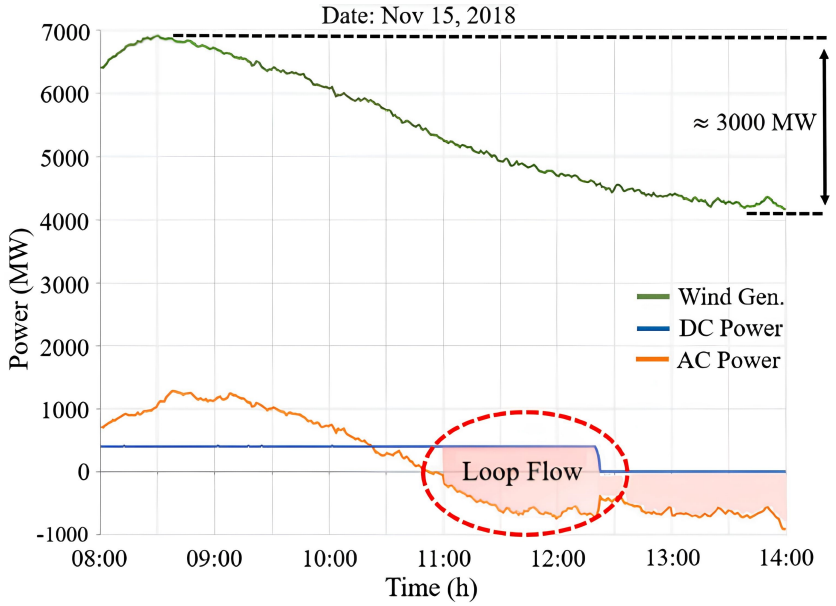

Figure 3: Loop flow in the Brazilian electrical power system. Adapted from [25].

The Northeast, with significant wind power, operates in parallel with Southeast and North connections. Due to the intermittency of renewable sources, abrupt reductions in wind generation can shift power flows unpredictably, leading to loop flow issues that require enhanced grid control

to prevent instability [26].

Brazil's power system integrates hydro, wind, and solar energy, facing challenges in transmission efficiency, load balancing, and reliability [27, 28]. While hydroelectricity remains the dominant source, its seasonal variability demands advanced control strategies to integrate intermittent renewables effectively [29, 30]. The increasing share of wind and solar generation has introduced new complexities, particularly in managing power distribution across geographically distant regions.

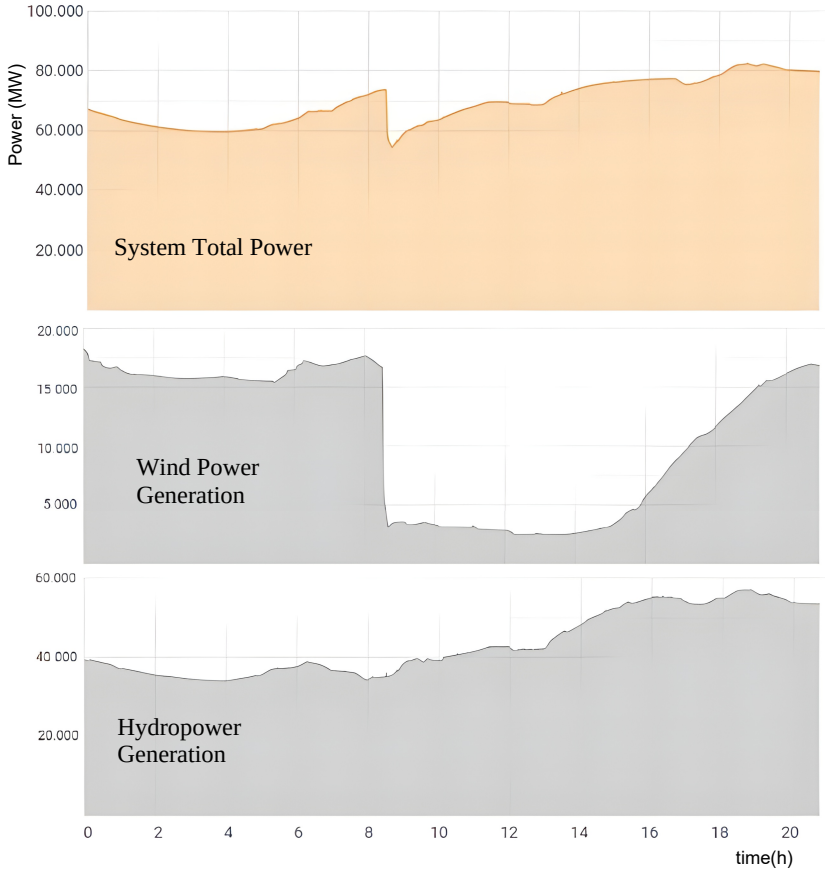

Figure 4: System generation behavior during the August 15, 2023 outage. Data source: [32].

Figure 4 further illustrates the impact of renewable intermittency on large-scale disturbances. The August 15, 2023 outage, triggered by transmission instability and protection system failures, mirrors key characteristics of the 2018 loop flow event. In both cases, sudden reductions in

wind generation led to shifts in transmission system loading, reinforcing the importance of optimized HVDC operation to prevent cascading failures and improve system resilience. These events highlight the need for more advanced control mechanisms to mitigate the negative effects of loop flow under increasing renewable penetration.

HVDC technology plays a critical role in addressing these challenges by enhancing power flow controllability and reducing regional imbalances [31]. However, seasonal fluctuations necessitate a flexible generation mix, with hydro and thermal power plants compensating for variations in renewable output. Additionally, the increasing penetration of HVDC links introduces unintended power circulation, known as loop flow, which can lead to inefficiencies and increased losses if not properly managed.

As Brazil's power system evolves, strategic HVDC deployment and advanced optimization techniques will be crucial for enhancing transmission efficiency, reliability, and renewable integration. The planned 2027 system expansion reflects these priorities, with an additional 4 GW of embedded HVDC capacity set to become operational within the next five years [33]. However, the integration of embedded HVDC links may exacerbate loop flow issues, requiring robust identification and mitigation strategies to avoid operational inefficiencies.

2.3 Models of HVDC

The models used in this work aim to analyze the impact of HVDC systems on power flow optimization and control. One of the key aspects studied in hybrid power networks is their role in improving stability, voltage regulation, and reactive power support. Proper modeling of these systems is essential to effectively manage power distribution, particularly in scenarios with a high share of renewable energy. To achieve this, the following steps are necessary:

- Model the electrical system components, including HVDC transmission links.

- Formulate the complete power flow equations and associated constraints for network operation and control.
- Ensure convergence and reliability of the models used.

A fundamental aspect of HVDC modeling is defining how the converters interact with the power grid. From the system's perspective, each HVDC connection point can be modeled as either a PQ or PV bus, depending on the control mode of the converter. In this study, the HVDC system is represented as a PV bus at connection points, as this configuration aligns best with the proposed power optimization methodology. This choice ensures more accurate control over active power injection while allowing reactive power compensation at the AC interface, improving system performance under varying load conditions.

Figures 5 and 6 illustrate the PQ and PV bus representations in the HVDC network.

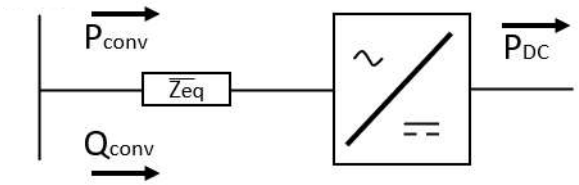

Figure 5: PQ bus connected to the HVDC link.

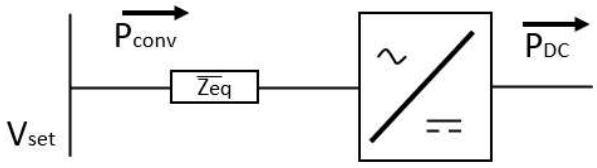

Figure 6: PV bus connected to the HVDC link.

The HVDC system can operate in three distinct control modes on its DC terminal: constant voltage, constant power, and voltage droop control. Each mode offers different trade-offs in terms of system stability

and control flexibility. In this work, the PV representation of HVDC connection points enables better power flow optimization by dynamically adapting to load variations while maintaining voltage stability.

In a system with multiple converters, one operates as the DC slack bus, ensuring power balance by compensating for transmission losses, as described in Equation 1.

$$P_{DC1} + P_{DC2} + ... + P_{DCN} - P_{DCL} = 0 \tag{1}$$

where P_{DCi} represents the power injected at each DC terminal, and P_{DCL} accounts for transmission losses in the network.

Figure 7 illustrates the constant voltage control mode, which ensures power balance within the DC system. The constant power mode, shown in Fig. 8, maintains a fixed power exchange, while voltage droop control, depicted in Fig. 9, allows flexible power sharing among converters, adapting dynamically to network conditions.

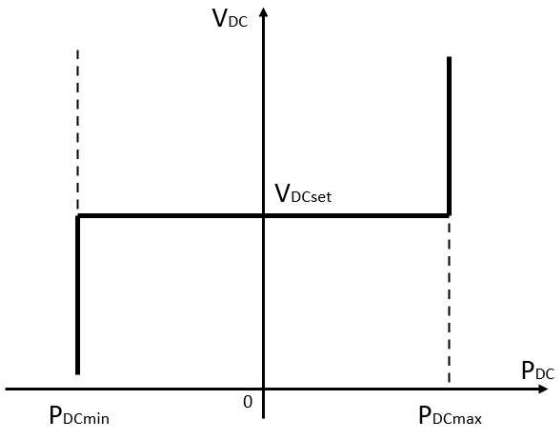

Figure 7: Constant voltage mode.

The voltage droop method follows a similar principle to frequency droop control in synchronous generators. Changes in DC voltage prompt HVDC stations to adjust power transmission accordingly, distributing power more efficiently across the network. Previous studies have validated this approach in line-commutated converter HVDC systems [34]

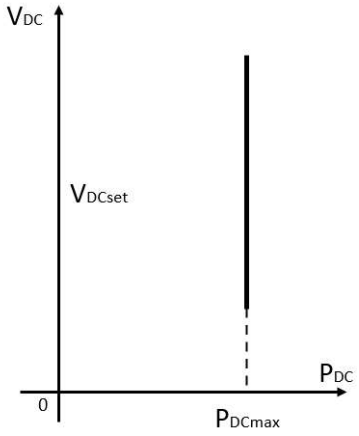

Figure 8: Constant power mode.

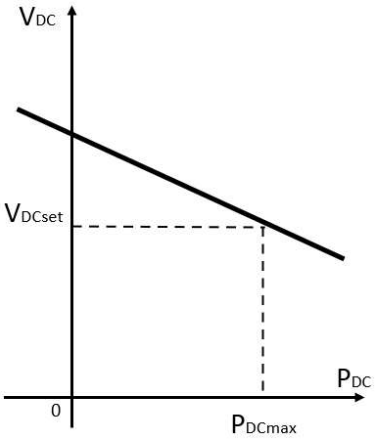

Figure 9: Voltage droop mode.

and later in voltage-source converter HVDC systems for offshore wind integration [35]. More recently, [36] proposed an optimized redistribution method to enhance AC grid frequency performance using a multi-terminal HVDC system.

By modeling HVDC links as PV buses in this study, it is ensured better alignment with the optimization framework for transmitted power. This approach enhances power flow predictability and network resilience,

particularly in the presence of renewable energy variability. The chosen representation also facilitates seamless integration of HVDC into hybrid networks, making it a key component of the proposed optimization methodology.

3 Sensitivity-Based Loop Flow Analysis

The analysis of power injections and their effects on network flow plays a fundamental role in ensuring the stability and efficiency of power systems. This chapter presents a sensitivity-based approach for loop flow analysis, focusing on the influence of power variations, particularly from HVDC links, on AC network behavior. By quantifying the impact of incremental changes in power injection on transmission paths, sensitivity analysis provides a systematic method for identifying and assessing loop flows.

3.1 Sensitivity analysis

Sensitivity analysis is a qualitative study designed to calculate sensitivity factors that illustrate how changes in control variables influence dependent variables within a system. In the context of power loop analysis, it is employed to assess how changes in power injection, particularly from HVDC systems, affect the power flow across the network. This type of analysis is used for understanding the interactions within the grid, especially in systems where HVDC links are embedded.

As detailed in [37], sensitivity analysis typically evaluates how power injection variations affect the flow between AC buses. This study focuses on assessing the influence of HVDC variations by examining the power injected into the network at buses connected to HVDC systems. The analysis keeps these variations small at each simulation step to maintain linearity and preserve the overall power balance of the system.

The system under consideration is characterized by a linear model represented as $I + \Delta I = Y(V + \Delta V)$. In this model, the current injection vector is denoted as I, ΔI represents the variation in injection current caused by HVDC perturbations, Y stands for the admittance matrix, and V symbolizes the voltage vector. Since the admittance matrix Y remains constant throughout the sensitivity analysis, variations in injected current result in changes to the voltage vector, subsequently influencing power flow between the buses.

Sensitivity analysis is conducted linearly, starting from the system's initial state. Notably, the sensitivity value remains linear in most cases, deviating from linearity only when nearing voltage collapse whereas analyzing branch power variations. This underscores the robustness and effectiveness of utilizing sensitivity analysis in this context. Although sensitivity analysis has long been a staple in the planning and operation of electrical systems, it has yet to be applied to the domain of loop flow identification, marking a novel application.

The analysis of AC power transmitted across branches concerning HVDC link variations fundamentally relies on understanding the cumulative effect of these variations at the points where the HVDC link is connected. Specifically, on Buses k, this variation is positive, denoted as $\partial P_{gk} = P_{gk} + \Delta P_{HVDC}$, whereas on Buses m, it is negative, expressed as $\partial P_{gm} = P_{gm} - \Delta P_{HVDC}$. This analysis rigorously maintains the balance between positive and negative variations, ensuring the total power balance within the system.

The ultimate goal of sensitivity analysis is to assess the consequences of HVDC variation on power flow within the AC network. This analysis allows the system operators to quantify the extent of influence exerted by HVDC changes on the broader power transmission system, providing valuable insights into loop flow.

In summary, sensitivity analysis emerges as a tool for investigating loop flow, enabling operators to check the impact of HVDC variations on the power flow of the AC network. This chapter establishes the foundation for a deeper understanding of loop flow in power systems, promising significant contributions to power system resilience and stability.

3.2 Modified Dijkstra's algorithm

This chapter presents a modified version of Dijkstra's algorithm tailored to identify the key path of loop flow induced by embedded High-Voltage Direct Current (HVDC) links within the power system. Unlike the traditional Dijkstra algorithm, which primarily considers the shortest path based on weight, this modified version incorporates impedance,

voltage, angular data, and power flow as part of its evaluation criteria. Additionally, sensitivity values are integrated to represent the influence of HVDC link transmission on each AC line in the power system. This enhancement allows the algorithm to prioritize the most critical lines within the network for monitoring and control, thus optimizing power system operations and bolstering resilience against disturbances.

The motivation behind modifying the Dijkstra algorithm stems from its application limitations in power systems, as discussed in [38]. The traditional algorithm's inability to handle digraphs effectively and its challenges with adjacent vertices in shortest path scenarios have been addressed by integrating sensitivity analysis and power flow considerations in this research.

The graph-based representation of the results, following a comprehensive sensitivity analysis, is crucial for efficient path identification and evaluation. The key branches of a power system, identified as segments with significant variations due to HVDC power level fluctuations, are highlighted in these graphs. These branches, often representing bottlenecks for system stability, require continuous monitoring. Identifying and optimizing these key branches is fundamental for understanding and mitigating the impact of loop flow within the power system.

Dijkstra's algorithm is a well-known shortest path algorithm that determines the minimum weight from a given starting node to all other nodes in a graph. The algorithm operates iteratively, updating weights based on the shortest known path at each step.

The process follows these steps:

- The starting node is initialized with a weight of zero, while all other nodes are assigned an initial weight of infinity, representing an unknown or unreachable state.
- At each iteration, the algorithm selects the node with the smallest known weight (initially the starting node), updates its status as "visited," and explores its adjacent nodes.
- For each adjacent node, the algorithm calculates the new potential

weight through the selected node and updates it if the new path is shorter than the weight recorded previously.

- This process continues until all nodes have been visited, ensuring that the shortest paths are determined efficiently.

In the context of power systems, the nodes in the algorithm represent electrical buses, while the edges correspond to the sensitivity values that quantify the impact of HVDC power variations on the AC grid. These values influence the algorithm's path selection, ensuring that the identified routes are not only the shortest in terms of lowest weight but also the most relevant for maintaining system stability.

Tables 1 and 2 illustrate the execution of the standard and modified Dijkstra algorithms, respectively. Each row corresponds to a bus in the system, and each column represents an iteration of the algorithm, showing how sensitivity values influence path selection.

Table 1: Iteration-by-iteration results of the standard Dijkstra algorithm.

Node	**Iteration 1**	**Iteration 2**	**Iteration 3**	**Iteration 4**	**Iteration 5**	**Iteration 6**
A	(0,A)					
B	(4,A)	(3,C)	(3,C)			
C	(2,A)	(2,A)				
D	(10,C)					
E	(12,C)	(8,B)		(8,B)		
F				(10,D)	(10,D)	
G				(14,D)	(12,E)	(12,E)

The modified version of the algorithm, as shown in Table 2, follows a similar step-by-step execution but incorporates sensitivity-based path selection. Instead of purely minimizing weight, the algorithm assigns priority to paths based on their influence on power system stability.

Key modifications include:

- Assigning higher weights to branches with greater sensitivity to HVDC fluctuations.

- Prioritizing key branches early in the search process to ensure critical paths are considered.
- Selecting paths that minimize power flow losses rather than just physical weight.

Table 2: Iteration-by-iteration results of the modified Dijkstra algorithm.

Node	**Iteration 1**	**Iteration 2**	**Iteration 3**	**Iteration 4**
A	(0,A)			
B	(4,A)	(3,C)		
C	(2,A)	(2,A)		
D	(10,C)			
E	(12,C)		(12,C)	
F		(14,F)		(14,F)

The results in Table 2 indicate a divergence in path selection compared to the standard approach in Table 1, emphasizing the influence of system sensitivity in defining optimal paths. While both algorithms identify shortest paths, the modified version prioritizes paths that have the greatest impact on loop flow, making it more suitable for power system applications.

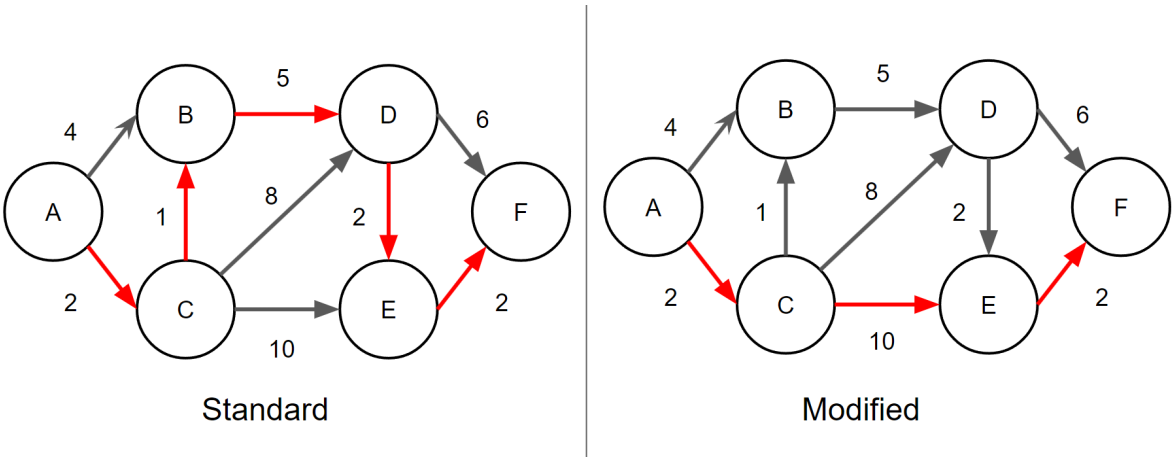

Figure 10: Dijkstra Algorithm visual example.

Figure 10 provides a comparison between the standard and modified versions of Dijkstra's algorithm, illustrating the determination of the shortest path between Buses A and F. Using the modified method, the key path changes, now passing through the connection between Bus C and E, identified as crucial in the initial step. The possible paths connecting points A and F are shown, with the key path highlighted in red for each methodology.

3.3 Detailed description of the algorithm, Step by Step

Step 1: Initialize the Graph.

The graph is initialized based on the specified sensitivity values. It is derived from the sensitivity matrix, which represents the variation in power transmitted in the HVDC across all branches of the AC network. Each row and column in this matrix corresponds to a bus, with rows indicating the "from bus" and columns indicating the "to bus." Each non-zero element in the sensitivity matrix signifies the sensitivity value of the power variation between the respective buses, forming a unidirectional edge.

Step 2: Identify the Most Sensitive Branch.

A sensitivity analysis is performed to identify the branch most affected by HVDC variations.

For the graph shown in Fig. 10, the branch with the highest sensitivity is C-E, with a sensitivity value of 10.

Step 3: Initialize Cost Estimates.

Cost estimates are initialized, where the estimate for the initial bus is set to zero, and all other buses are assigned an estimate of infinity, designating them as open buses. Precedents for each bus are also assigned in this step, tracking the preceding bus on the least-cost path.

The algorithm iteratively adjusts the cost estimates associated with each open bus, as shown by Algorithm 1.

Algorithms 1 and 2 are presented in pseudocode to ensure clarity and facilitate implementation across various programming environments, enhancing accessibility for researchers. The pseudocode format follows

a Python-like structure, chosen for its readability and wide familiarity among researchers.

Algorithm 1: Dijkstra's Algorithm

input : Graph G, Start Vertex s
output: Shortest Path from s to all other vertices

```
Function Dijkstra(G, s)
    distances ← dictionary with default value ∞
    previous_vertices ← empty dictionary
    distances[s] ← 0
    priority_queue ← new PriorityQueue
    priority_queue.push(s, 0)
    while priority_queue is not empty do
        current_vertex ← priority_queue.pop()
        for each neighbor, weight in G[current_vertex].items() do
            alt ← distances[current_vertex] + weight
            if alt < distances[neighbor] then
                distances[neighbor] ← alt
                previous_vertices[neighbor] ← current_vertex
                priority_queue.push(neighbor, alt)
            end
        end
    end
    path ← empty list
    current_vertex ← end_vertex
    while current_vertex is defined do
        path.insert(0, current_vertex)
        current_vertex ← previous_vertices[current_vertex]
    end
    return path
```

Standard Dijkstra's algorithm is adjusted to ensure that the shortest paths pass through the most sensitive branch.

Step 4: Modified Dijkstra's Algorithm.

The modified Dijkstra's algorithm identifies the shortest path from node A to node F, passing through the most sensitive branch C-E, as shown in Algorithm 2. The algorithm determines the shortest path for the first segment from A to C with a weight of 2. For the second segment from E to F with a weight of 2.

Algorithm 2: Modified Dijkstra's Algorithm

input : Graph G, Start Vertex s, End Vertex t
output: Shortest Path from s to t passing through the most sensitive branch

Function `ModifiedDijkstra`(G, s, t)
  $most\_sensitive\_branch \leftarrow$ `IdentifyMostSensitiveBranch`(G)
  $from\_msb, to\_msb \leftarrow most\_sensitive\_branch$
  $path1 \leftarrow$ `Dijkstra`$(G, s, from\_msb)$
  $path2 \leftarrow$ `Dijkstra`(G, to_msb, t)
  $combined\_path \leftarrow path1 + [to\_msb] + path2[1:]$
  return $combined\_path$

Step 5: Path Construction.

After processing all buses, the path is constructed by tracing back from the destination bus to the initial bus, following the precedents assigned in Step 3. In this process, branches with low sensitivity are filtered out, ensuring that only the most sensitive branches to HVDC variations are included in the final path.

Thus, the complete path from Ⓐ → Ⓒ → Ⓔ → Ⓕ found by the proposed modified Dijkstra's algorithm is shown in Fig. 10, with a total weight of $2 + 10 + 2 = 14$. This path guarantees that the most sensitive branch is included, optimizing network monitoring and control for HVDC variations.

From a physical perspective, the traditional algorithm treats the power grid as a static network, focusing solely on structural aspects. The improved algorithm, however, views the grid dynamically, accounting for real-time operational conditions. This dynamic approach considers the impact of load changes, generation shifts, and HVDC power variations, aligning the algorithm more closely with the actual operational realities of a modern, integrated power system.

In summary, the proposed modified Dijkstra's Algorithm is a powerful tool that integrates sensitivity-based analysis and traditional pathfinding techniques to identify and optimize the key path for loop flow analysis within the power system. This innovative approach offers a more comprehensive understanding of loop flow and contributes to the enhanced

resilience and stability of the power grid.

3.4 Numerical example of the loop flow identification

This chapter shows examples of the application of the loop flow identification process, using the IEEE test systems of 4, 14, 57, and 118 buses.

3.4.1 Identification of Loop Flow Paths in the IEEE 4-Bus Test System

The IEEE 4-bus test system was chosen as the first example due to its small size, allowing for a clear analysis of loop flows. An HVDC link was added to the system, connecting buses 2 and 4. Bus 1 was defined as the swing bus, while bus 4 was modified to a PV-type bus. Figure 11 presents the single-line diagram of the adapted test system, and the corresponding data is provided in Table 8.

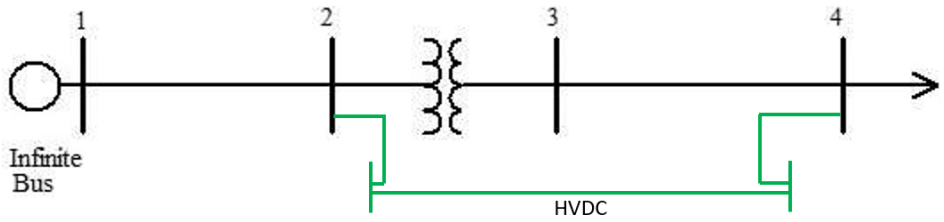

Figure 11: Adapted IEEE 4-bus test system.

Table 3 shows the results of the sensitivity analysis with the HVDC link connecting buses 2 and 4. Given the system's small size, it is possible to observe the return path of the excess power flow, which follows the sequence: $4 \rightarrow 3 \rightarrow 2$. Figure 12 presents the data in graph form, highlighting the identified branches. Using the methodology described in Chapter 3, the same path for excess power flow is obtained, confirming the presence of a potential loop flow. In future stages of this study, further analysis will determine whether loop flow is actively occurring.

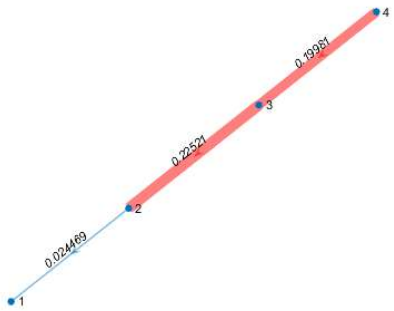

Figure 12: Graph representation of the IEEE 4-bus test system.

Table 3: Sensitivity analysis results for the IEEE 4-bus test system

From	To	Sensitivity
2	1	0.024469
3	2	0.225209
4	3	0.199807

3.4.2 Identification of Loop Flow Paths in the IEEE 14-Bus Test System

The second example used was the IEEE 14-bus system, a well-known and widely used test system, and easy to visualize given its small number of buses. An HVDC link was added to this system, connecting buses 2 and 9, while bus 1 is the swing bus. Figure 13 shows the single-line diagram with the HVDC connection highlighted in green. The system data and branch parameters are presented in Tables 10 and 11, respectively.

The data of the sensitivity analysis of the power flow between branches of the system with respect to the transmitted power is shown in Table 4. In the first case, a line opening was considered between buses 2 and 4, and in the second case, a line opening was considered in the branch between buses 6 and 5.

Figure 14 shows the results of the sensitivity analysis in the form of graphs and the most relevant path highlighted in red. Eight paths are found connecting buses 2 and 9, which are:

1. [9-4-2]

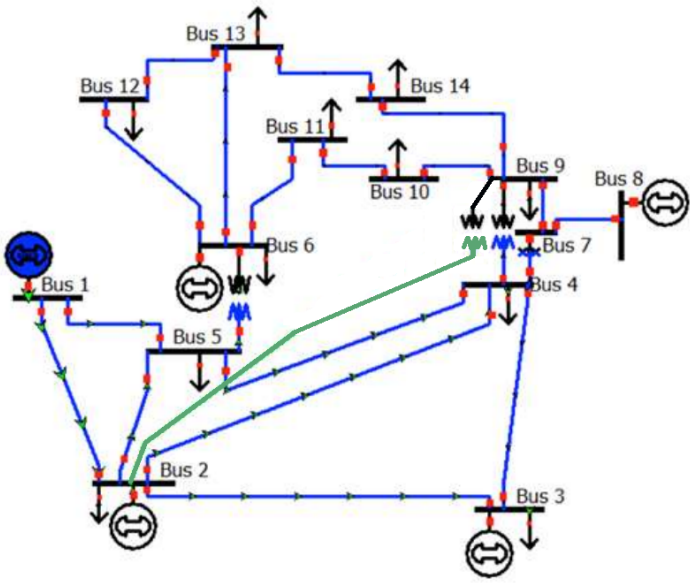

Figure 13: IEEE 14-Bus adapted test system with an HVDC connecting buses 9 and 2.

Table 4: IEEE 14-Bus Results

Line opening 2 to 4			Line opening 6 to 5		
From	To	Sensitivity	From	To	Sensitivity
1	2	0.0469	1	2	0.0236
1	5	0.0627	3	2	0.0433
2	3	0.0628	4	2	0.0782
2	4	0.0000	4	3	0.0405
2	5	0.0936	4	5	0.0863
3	4	0.0579	5	1	0.0366
4	5	0.0829	5	2	0.0567
4	7	0.0905	6	5	0.0000
4	9	0.0511	7	4	0.1286
5	6	0.0592	7	8	0.0000
6	11	0.0360	9	4	0.0725
6	12	0.0046	9	7	0.1286
6	13	0.0186	10	9	0.0006
7	8	0.0000	14	9	0.0005
7	9	0.0905	11	10	0.0004
9	10	0.0356	6	11	0.0001
9	14	0.0228	12	6	0.0000
10	11	0.0355	13	6	0.0000
12	13	0.0045	13	12	0.0000
13	14	0.0227	14	13	0.0000

2. [9-4-3-2]
3. [9-4-5-1-2]
4. [9-4-5-2]
5. [9-7-4-2]
6. [9-7-4-3-2]
7. [9-7-4-5-1-2]
8. [9-7-4-5-2]

The most relevant path for a loop flow analysis, according to the system sensitivity-based methodology proposed in this Ph.D. Thesis is the fifth one, i.e. [9-7-4-2], which contains the most critical branches defined during the identification step, shown in Table 4. For case 01 the path found is [9-4-5-2], which contains the most critical branch, 2 to 5.

3.4.3 IEEE 57-Bus System with HVDC Integration: Sensitivity Analysis and Line Openings

The IEEE 57-Bus test system [43], representing the U.S. Midwest Power system in the 1960s, was selected due to its complexity and widespread use in power system research. Similar to the Brazilian power system, it features a meshed electrical network, making it ideal for examining Loop Flow phenomena using the modified Dijkstra Method proposed here. An embedded HVDC link was added, connecting Buses 20 and 3, highlighted in green in Fig. 15. The system's bus data and branch parameters are detailed in Tables 12 and 13, respectively.

Two cases were created using the IEEE 57-Bus system. In Case 01, a line opening between Buses 22 and 38 is considered, and in Case 02, a line opening between Buses 38 and 48 is examined. These buses were chosen for their location and because they are among the most sensitive in the base case, with the branch between Buses 22 and 38 having a sensitivity of 0.2591 p.u., and the branch between Buses 38 and 48 having a sensitivity of 0.1126 p.u.

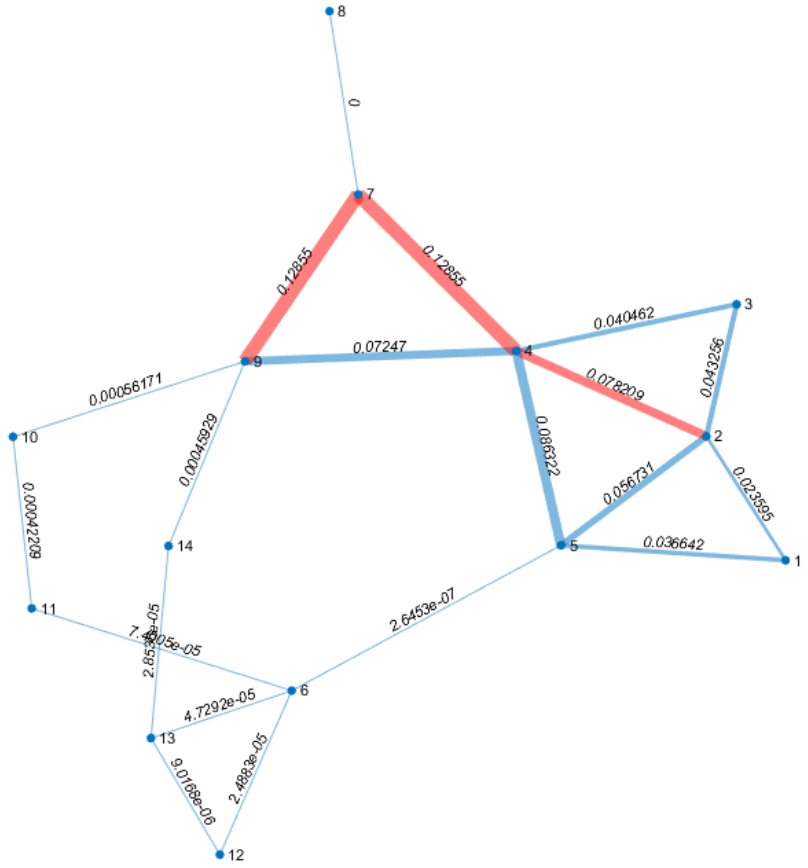

Figure 14: IEEE 14 bus with line opening between buses 6 and 5 graphs.

When these lines are opened, the power flow that was previously carried by these branches must be redistributed throughout the system. This redistribution can potentially overload other transmission lines, pushing them closer to their thermal and power transmission limits. Such conditions highlight the importance of the modified Dijkstra method, which identifies critical paths and helps anticipate potential overloads or risks of instability within the system.

The methodology presented here is crucial for visualizing how the system reacts to these contingencies, providing insights into the operational resilience of the system in the face of significant power flow changes due to HVDC integration.

Table 5 ranks the key branches obtained from the sensitivity analysis

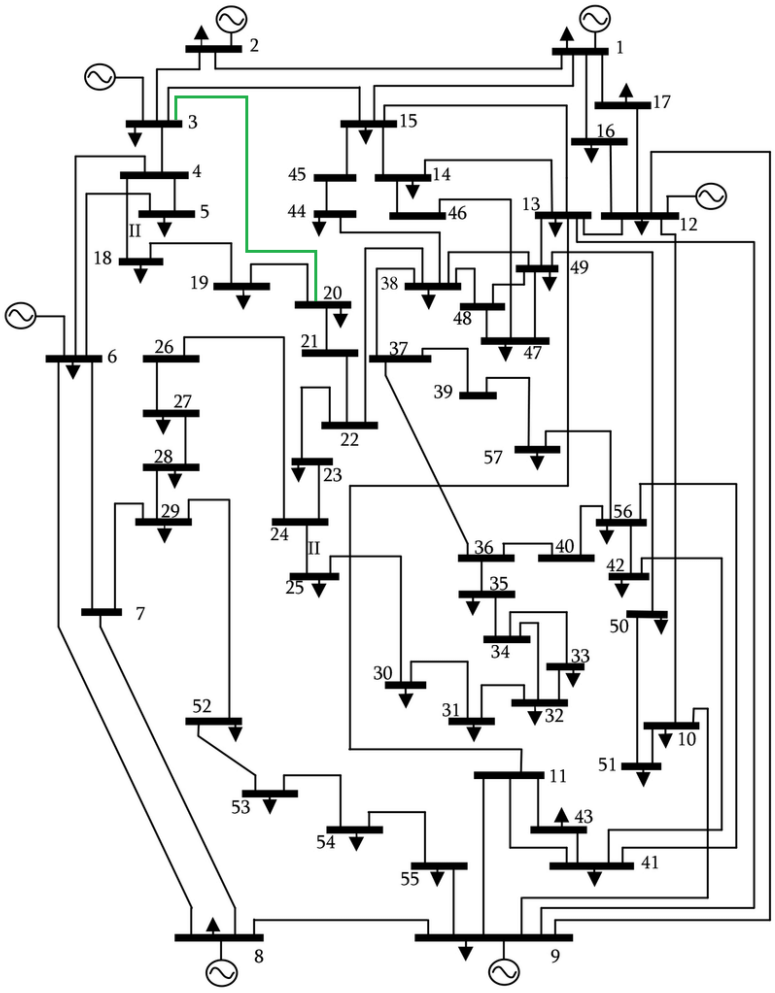

Figure 15: IEEE 57-Bus test system with an HVDC connection between Buses 20 and 3.

for both cases, demonstrating how changes in system topology influence sensitivity analysis results. The most sensitive branch is then used to close the loop flow, guiding the selection of paths for further analysis.

The key paths identified by the modified Dijkstra algorithm for Case 01 and Case 02 are shown in Figures 16 and 17, respectively. These key paths represent the shortest paths that include the branches most sensitive to HVDC variations. The red arrows in the figures highlight the key path identified by the algorithm, while the green arrow marks the connection point of the simulated HVDC.

Table 5: Key Branches Sensitivity Analysis for IEEE 57-Bus System

Case 01			**Case 02**		
From	To	Sensitivity Index	From	To	Sensitivity Index
4	3	0.3283	20	21	0.2935
20	19	0.2562	21	22	0.2935
18	4	0.2388	22	38	0.2440
19	18	0.2388	4	3	0.2309
20	21	0.2282	15	3	0.1987
21	22	0.2281	20	19	0.1948
22	23	0.2233	18	4	0.1820
23	24	0.2227	19	18	0.1820
28	29	0.1929	45	15	0.1245
27	28	0.1883	44	45	0.1182

The modified Dijkstra algorithm differs from the traditional approach by integrating sensitivity analysis, which allows it to identify paths that are not only shortest in weight but also most critical in terms of system dynamics.

In [6], tests conducted with the IEEE 57-Bus system identified loop flows in the AC network. Loop number 15, as cited in the reference, includes the buses connected by the HVDC link simulated in this examples (Buses 3 and 20). This specific path was chosen for comparison because it encompasses the critical branches connected by the HVDC link. The complete path identified by [6] was: (38) → (22) → (21) → (20) → (19) → (18) → (04) → (03) → (15) → (14) → (46) → (47) → (48) → (38).

For this study, the paths identified using the modified Dijkstra algorithm were:

- Case 1: (20) → (19) → (18) → (04) → (03)
- Case 2: (20) → (21) → (22) → (38) → (44) → (45) → (15) → (03)

The inclusion of sensitivity analysis in the modified algorithm offers a more dynamic and accurate reflection of the system's operational realities, providing better tools for monitoring and controlling HVDC-induced loop flows in complex power networks.

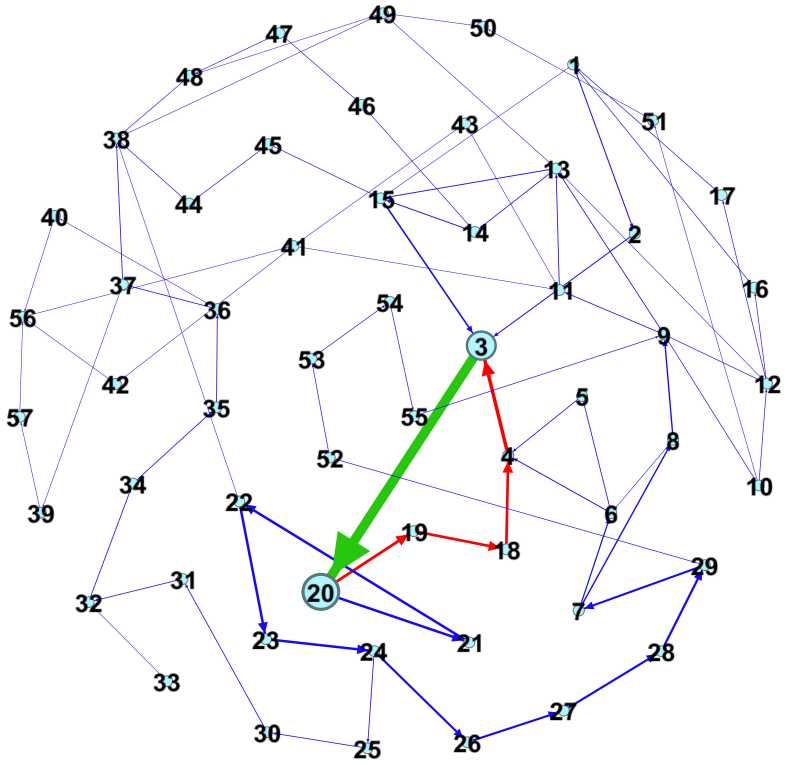

Figure 16: Key path identified in Case 01 using the IEEE 57-Bus test system.

3.4.4 Sensitivity Analysis and Path Identification in the IEEE 118 Bus System with Embedded HVDC Links

The IEEE 118 bus test case represents an approximation of the U.S. Midwest Power system as it was in December 1962 [43]. This system contains 19 generators, 35 synchronous condensers, 177 lines, 9 transformers, and 91 loads. The HVDC was added connecting Buses 20 and 3, which were chosen due to the distance between them and the fact that both buses have generation and load. This setup allows for the analysis of power variation transmitted in the HVDC in both directions. The system's bus and branch data are presented in Tables 14 and 15, respectively.

Due to the large number of interconnections between the buses in this example, the use of sensitivity analysis to define the possible paths of the loop flow is essential, since the number of branches that the loop forms

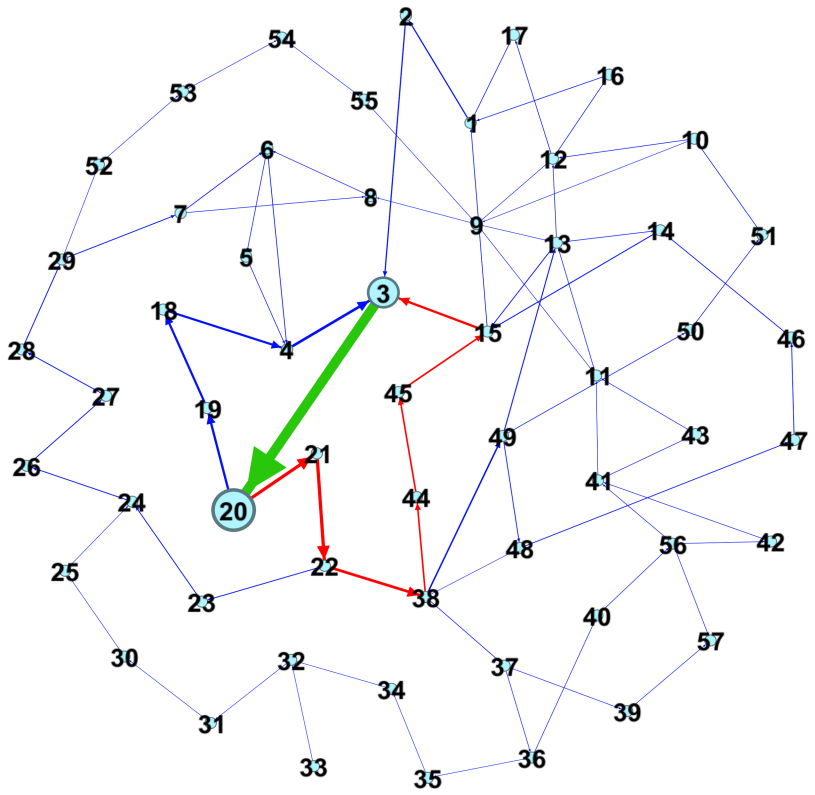

Figure 17: Key path identified in Case 02 using the IEEE 57-Bus test system.

Table 6: IEEE 118 Bus sensitive analysis results

IEEE188 Base case			Line opening 5 to 8		
From	To	Sensitivity	From	To	Sensitivity
20	19	0.36859	19	20	0.39342
30	8	0.25702	15	19	0.30996
8	5	0.25702	16	17	0.23401
5	3	0.23393	12	16	0.21241
19	15	0.22187	3	5	0.20559
12	3	0.14914	14	15	0.19444
22	23	0.12892	17	30	0.1934
21	22	0.12678	65	68	0.19148
20	21	0.12564	68	69	0.18553
12	2	0.11697	12	14	0.1793

is substantially larger than in the previous example, making a ranking necessary to define which branches are more influenced when variations in the power transmitted in the HVDC occur.

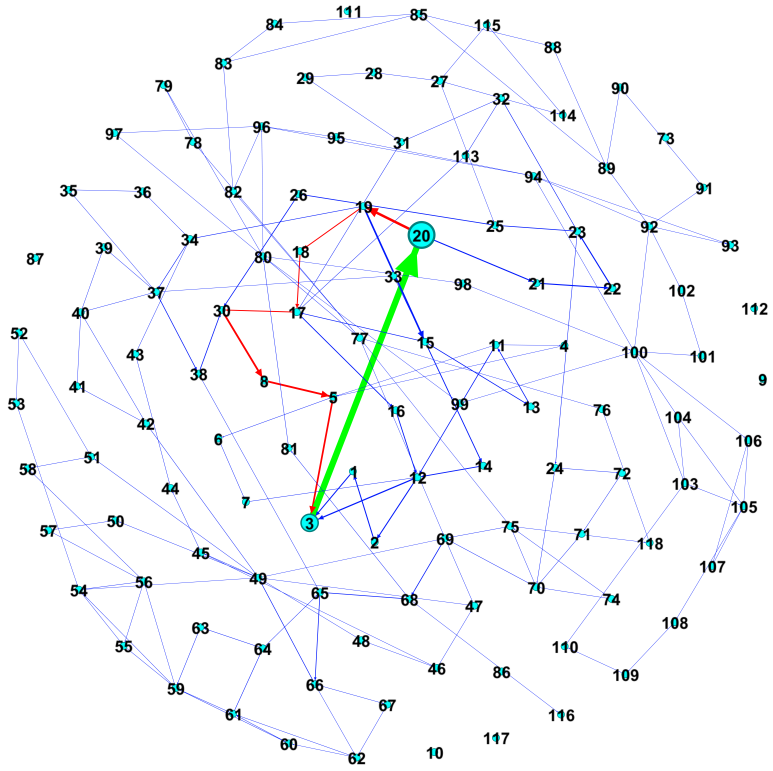

Figure 18: IEEE118 bus base case graphs.

The sensitivity analysis results are summarized in Table 6. In the base case, a total of 14,380 paths were identified connecting Buses 3 and 20. The most sensitive branches in this scenario were 20 to 19, 30 to 8, 8 to 5, and 5 to 3. Using the proposed methodology, the most critical path was determined as:

(03) → (01) → (02) → (12) → (07) → (06) → (05) → (08) → (30) → (17) → (15) → (19) → (20).

Although multiple highly sensitive branches were identified, the algorithm prioritizes the most critical path in the current step. However, these additional sensitive branches can be utilized in future iterations to define new priority paths, enabling the identification of alternative routes under different operating conditions.

For the scenario with the line opening between Buses 5 and 8, a total of 9,095 paths were found. In this case, the most sensitive branches were 20 to 19, 19 to 15, 17 to 16, and 16 to 12. The identified critical path for

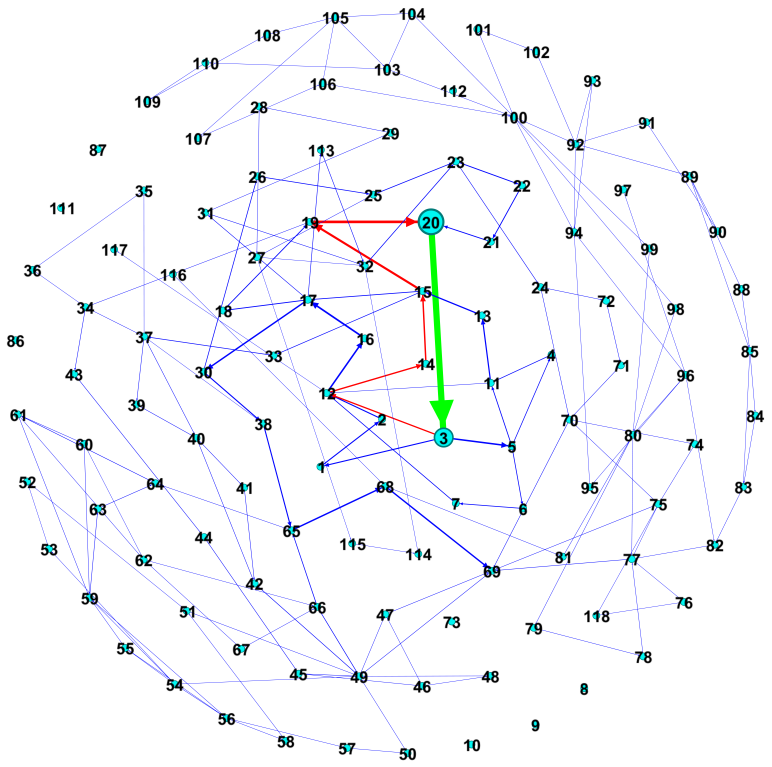

Figure 19: Graphs of IEEE 118 bus line open between Bus 5 and 8.

this scenario was:

(03) → (01) → (02) → (12) → (16) → (17) → (18) → (19) → (20).

As in the base case, only the most critical path is selected for analysis, but the identified sensitive branches can serve as key candidates for future assessments, potentially revealing alternative paths based on changing system conditions.

Figures 18 and 19 display the sensitivity graphs for HVDC variation. The path identified by the algorithm is highlighted in red, while the simulated HVDC is marked in green. Comparing the figures reveals the impact of opening the line between Buses 8 and 5, which alters the network configuration and the identified key path.

In Fig. 20, compared to Figures 18 and 19, a filter is applied to exclude branches with sensitivities below 5% of the maximum value, as explained in 3.3. In Step 5, Path Construction, after identifying the

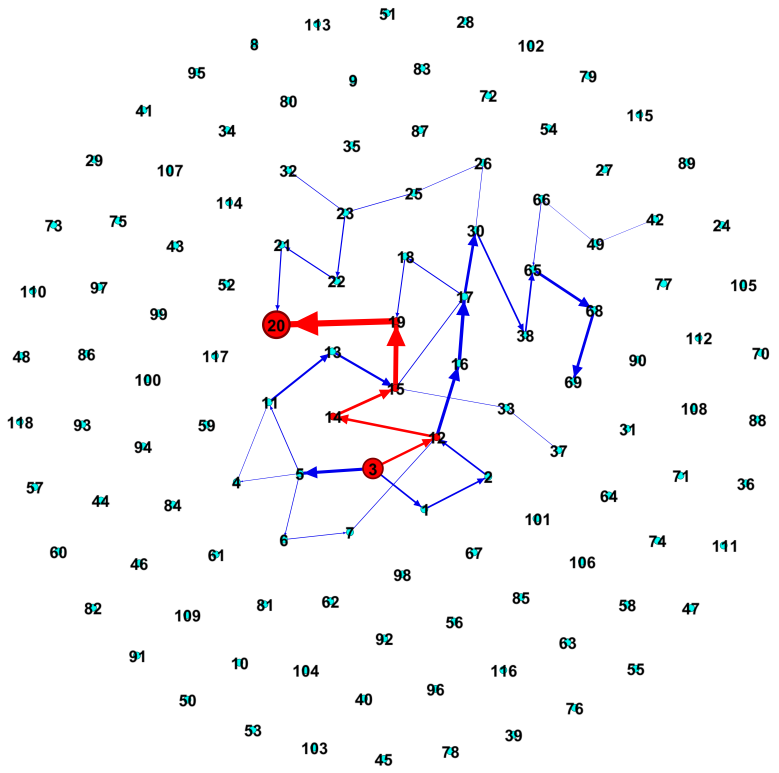

Figure 20: Graphs of IEEE 118 bus line open between Bus 5 and 8, after the filter.

paths, branches with low sensitivity are filtered out, which reduces the number of branches analyzed and enhances the efficiency of the overall process. As a result, although the red lines appear to go through the same nodes, the nodes have been repositioned to reflect only the most critical connections. The resulting graph emphasizes the reduction in the number of AC system branches, while the HVDC link continues to connect buses 3 and 20, maintaining its role in the system.

4 Analysis of HVDC Induced Loop Flow

The analysis of active power flow variation induced by HVDC transmission employs the continuation method, which consists of two main steps: prediction and correction. In the prediction step, a variation parameter, λ, is introduced into the power flow equations to represent the increase in power transmitted through the HVDC system. This parameter increases incrementally until either the HVDC reaches its operational limits or the power flow simulation fails to converge.

The tangent vector method [44] plays a key role in determining the direction and sensitivity of the system's state variables concerning the variation in λ. The tangent vector (TV) provides insights into the expected change in power flow as λ increases, as expressed in Eq. (2).

The power flow equation with the inclusion of λ is defined as:

$$P_k(V, \theta) - P_{km}(V, \theta, \lambda) - P_{HVDC}(\lambda) = 0, \tag{2}$$

where:

- $P_k(V, \theta)$ denotes the active power at bus k, dependent on voltage magnitude V and phase angle θ.
- $P_{km}(V, \theta, \lambda)$ is the active power flow between buses k and m, which also depends on V, θ, and λ.
- $P_{HVDC}(\lambda)$ represents the power transmitted through the HVDC link as a function of λ.

The variation parameter λ is determined using the equation:

$$\lambda = \frac{\rho_1}{||TV||}, \tag{3}$$

where:

- ρ_1 is a predefined step coefficient that controls the magnitude of the parameter increment.

- $||TV||$ is the norm of the tangent vector, ensuring λ is scaled appropriately according to system sensitivity.

The tangent vector TV is derived from the following expression:

$$TV = J^{-1} \begin{pmatrix} \frac{\partial P}{\partial \lambda} \\ \frac{\partial Q}{\partial \lambda} \end{pmatrix}, \tag{4}$$

where:

- J is the Jacobian matrix of the power flow equations, containing the partial derivatives of active power P and reactive power Q with respect to the state variables.
- $\frac{\partial P}{\partial \lambda}$ and $\frac{\partial Q}{\partial \lambda}$ represent the sensitivity of the active and reactive power flows to changes in λ.

The prediction step, guided by the tangent vector, efficiently estimates the direction and magnitude of the next state in the continuation method. This approach is particularly valuable in identifying critical points in the power system, such as those leading to loop flows.

In the correction step, the method adjusts the voltage and power values to satisfy the power flow equations for the new value of λ. This adjustment refines the estimated system state, leading to a valid and convergent solution. The continuation method, illustrated in Fig. 21, identifies the power flow reversal point, which is essential for analyzing HVDC-induced loop flows. The figure was generated through simulations of the Brazilian 107-Bus system, analyzing the variation in power transmitted on the AC line between buses 360 and 325, which will be further examined in this paper.

This method utilizes the tangent vector to enhance the efficiency and accuracy of loop flow analysis, offering a detailed approach to managing the complexities of power system dynamics, particularly when integrating HVDC transmission links.

The correction process, informed by the prediction, plays a crucial role in accurately determining changes in the transmission direction. This

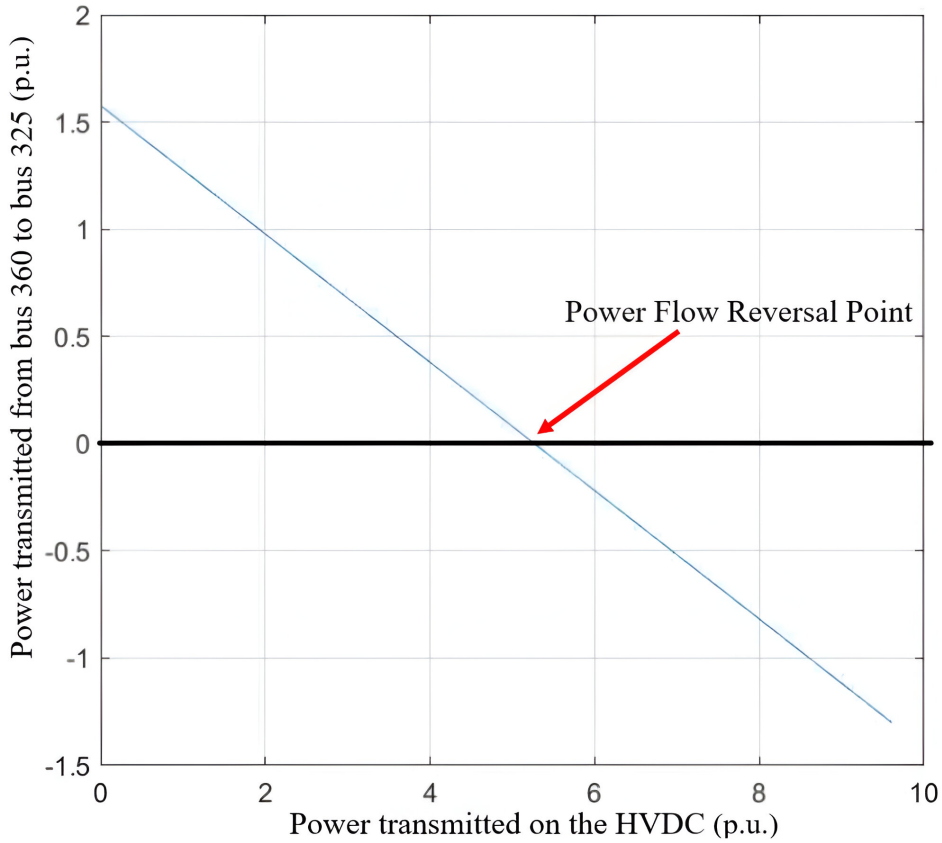

Figure 21: Analysis of HVDC Induced Loop Flow.

process, integral to the Newton-Raphson method, ensures robust convergence and enhances the overall reliability and stability of the power system during HVDC-induced variations.

4.1 Impact of HVDC Losses on Loop Flow

Loss analysis is crucial in optimizing loop flow, as HVDC transmission systems face various losses, including resistive, converter, and transmission losses. These losses can be categorized as linear or quadratic based on their relationship with transmitted power [45].

Linear converter losses arise from the AC/DC conversion process, remaining relatively constant and unaffected by transmission levels. Examples include hight switching losses in converter valves and losses in

transformers [46].

Resistive losses, exhibiting a quadratic behavior, arise from the resistance in the transmission line, including conductor resistance, grounding resistance, and contact resistance.

The total losses of the HVDC transmission can be modeled by (5), where:

$$P_{DC_{losses}} = \sigma + \gamma\lambda \tag{5}$$

σ represents the fixed losses of the embedded HVDC link, and γ indicates the coefficient of losses related to the power transmitted by the HVDC, λ, as specified in (2).

In contrast, quadratic transmission losses increase as transmitted power increase. These losses, varying with the square of transmitted power, result from leakage reactance, dielectric losses, and losses in insulating materials.

Equation (6) indicates the sum of losses in the AC line of the system, where, $m \in \phi_k$, and ϕ_k is the list of adjacent busses of bus k, V_k and V_m are the voltage magnitude of the AC buses, G_{km} is the value of the conductance of the AC line km.

$$P_{AC_{losses}} = \sum_k \sum_m G_{km}(V_k^2 + V_m^2 - 2V_k V_m cos(\theta_{km})) \tag{6}$$

Minimizing losses in transmission systems with embedded HVDC is essential to enhance efficiency and reduce costs. Various measures can be taken, such as selecting optimal transformer designs, improving converter efficiency, and implementing advanced control strategies.

$$\frac{dP_{total}}{d\lambda} = \sum_k \sum_m 2G_{km}(\frac{dV_k}{d\lambda} + \frac{dV_m}{d\lambda} - \frac{dV_k V_m cos(\theta_{km})}{d\lambda}) + \gamma \tag{7}$$

Equation (7) shows the variation of active power concerning the power change in the HVDC. When the function's derivative equals zero, it marks the minimum point for losses. The transmission loss coefficient

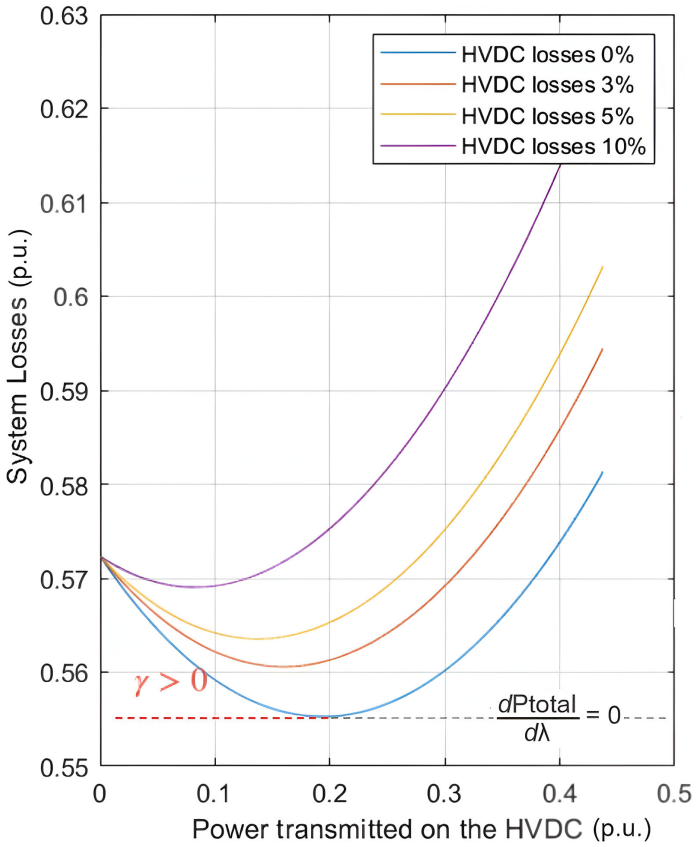

Figure 22: Total losses.

of HVDC, denoted by γ, shifts this minimum point to the left on the graph, as depicted in Fig. 22.

Analyzing system losses aids in identifying the moment of loop flow occurrence. Figure 22 visually represents total losses in the system for different loss values adopted in the HVDC during increased power transmission. When HVDC loss is considered 0%, shown in blue in Fig. 22, the losses in the system are exclusively those in the AC system. In this simulation, the increase in power transmitted by the HVDC link incurs lower losses than the AC system. Therefore, the total losses should always decrease, but at a point, they start to rise again due to Loop Flow. This occurs because the extra power transmitted on the HVDC link circulates through the AC system, returning to the point of origin and its surroundings. The minimum point of the curve indicates the beginning

of loop flow. Adopting higher loss values for HVDC transmission shifts this point to the left because HVDC losses are linear and increase proportionally with transmitted power.

Figure 23 displays the power transmitted on the line connecting Buses 18 and 19 of the IEEE 57 bus system. Flow inversion occurs when the power transmitted in the HVDC exceeds 0.11 pu, indicating a local effect of loop flow. Whereas Fig. 22 indicates the effect globally, Fig. 23 provides insight into the local impact of loop flow. This comprehensive approach ensures a thorough understanding of loop flow dynamics, aiding in the efficient management and optimization of HVDC transmission systems, as mentioned in Contribution 2 in Chapter 1.

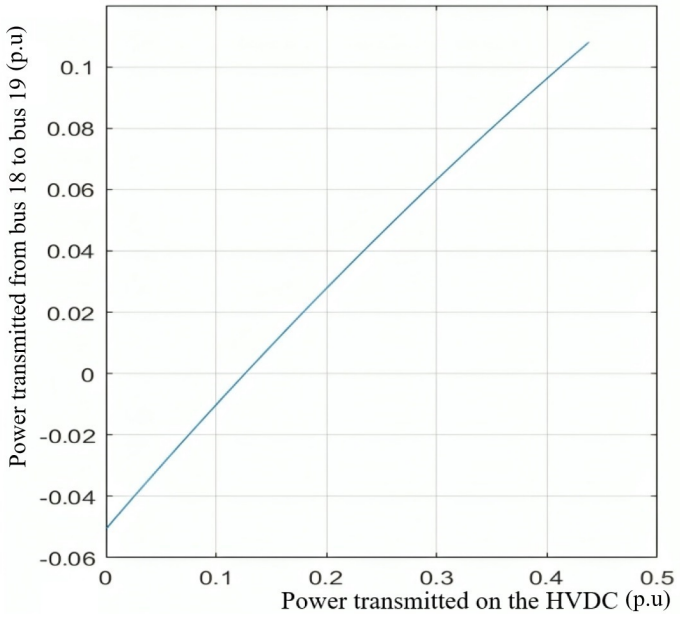

Figure 23: Active power flow between Buses 18 and 19 with HVDC between Buses 3 and 20.

4.2 Case Study: Loop Flow in an IEEE 57-Bus System

This chapter presents examples of loop flow analysis using the IEEE 57 bus test system. In this scenario, HVDC is introduced between Buses 3 and 20, with Bus 20 in the central region, as shown by Fig. 15.

Through the identification process, the key branch for analysis is the one between Buses 20 and 21. Figure 24 illustrates the variation of

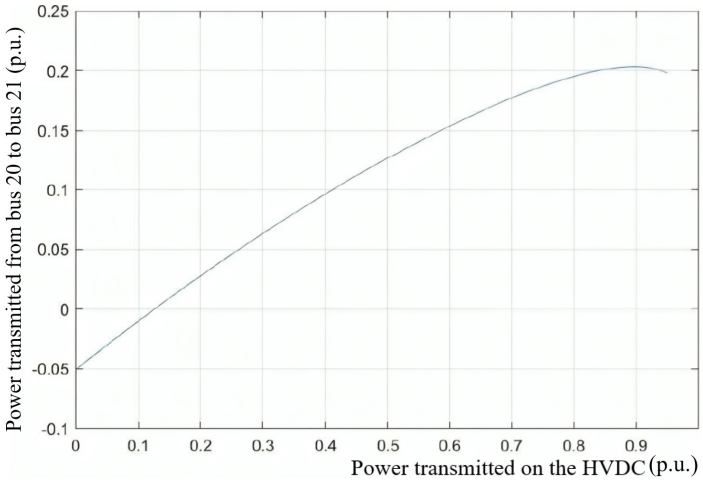

Figure 24: Active power flow between Buses 20 and 21 with HVDC between Buses 3 and 20.

transmitted power in the embedded HVDC link and its impact on power between the branches. In this context, P_{km}, where km is a subscript denoting the specific pair of buses under consideration, represents the power at the analyzed bus. For this example, P_{km} refers to the power flow between Buses 20 and 21.

The flow direction between Buses 20 and 21 undergoes a reversal when the simulated transmission in the HVDC exceeds 0.126 pu. Beyond this threshold, loop flow induced by the HVDC becomes apparent, and its magnitude steadily rises until it reaches the limit value of 0.95 pu, as outlined in Contribution 3 in Chapter 1.

Figure 24 also illustrates that adopting a power reference direction in a branch can result in a negative initial value. However, the methodology continues to identify variations in flow direction, transitioning from negative to positive in this scenario.

4.3 Impact of System Conditions on HVDC-Induced Loop Flow

In this chapter, the IEEE 57-Bus system was used, and new load and generation conditions were created; the HVDC is connected between buses 20 and 3. Table 7 summarizes the changes made in each case, whereas Fig. 25 shows the difference of the transmission curves of active power in the line between buses.

Table 7: Simulated cases of the IEEE 57-Bus system

Case	Changes
1	Base case
2	Increase of generation at Bus 12 and load at Bus 38, by 1.0 pu
3	Increase of generation at Bus 12 and load at Bus 21, by 1.0 pu
4	Change of 0.5 pu of load from Bus 12 to Bus 20

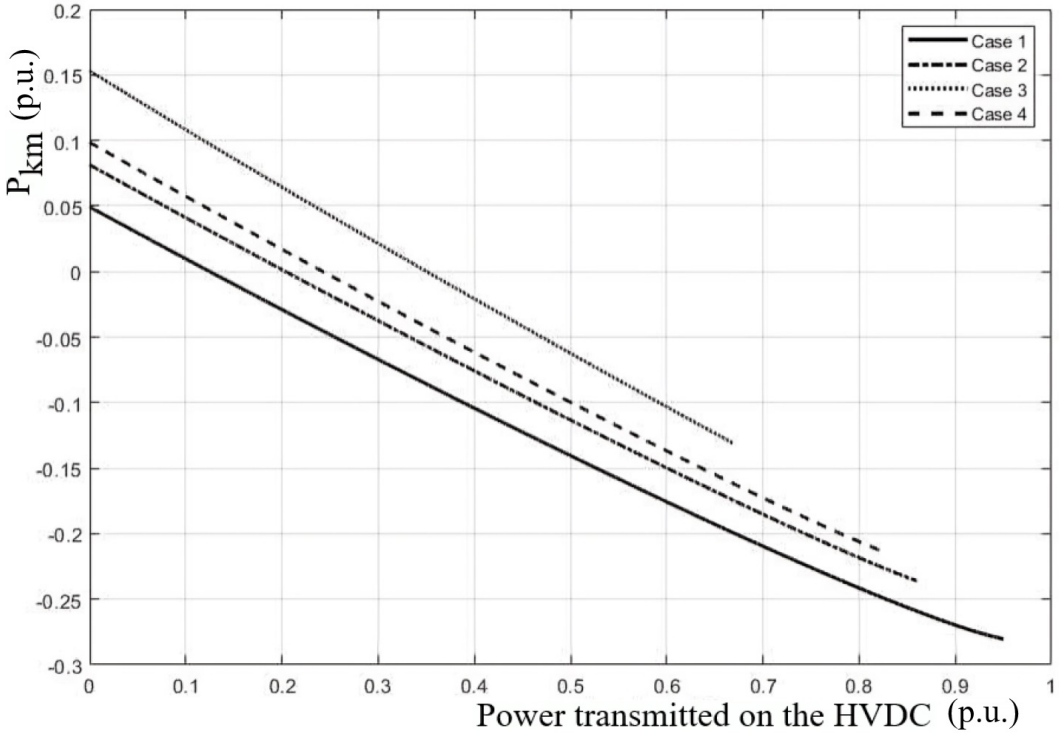

Figure 25: Comparison between cases.

Figure 25 illustrates the significant impacts on the maximum achievable transmission value on the line, before causing a flow reversal on the analyzed line, due to changes between the cases outlined in Table 7. In the base case, loop flow initiates with 0.126 pu transmitted on the HVDC line. In case 4, involving a load shift of 0.5 pu from Bus 12 to 20, the value increases, and the loop flow initiates with 0.23 pu. This variation can be used as an alert, and an additional safety parameter for the operator, as detailed in Contribution 4 in Chapter 1. Identifying key paths that require monitoring during HVDC power variations makes the modified Dijkstra's algorithm particularly useful for real-time

applications and contingency planning.

4.4 Case Study: HVDC Loop Flow in the 107-Bus System

The 107-Bus test system represents the South-Southeast and Mato Grosso regions of the Brazilian National Interconnected System. Data for the 107-Bus system used in this study were extracted from [47]. The system data and branch parameters are presented in Tables 16 and 17, respectively.

This system was selected due to the high number of generation units and loads in the region, which features many connections and a meshed transmission network. An HVDC link was introduced between buses 325 and 535, as depicted in Figures 26 and 28. These buses were chosen for their strategic location and because they are connected to generation, enabling sensitivity analysis in both directions of HVDC power transmission.

The inclusion of an HVDC link in this system is critical for investigating the effects of power transmission in loop flow scenarios. The study focuses on identifying and analyzing these loop flow events, which are caused by power transmission through the HVDC and can significantly impact the performance and stability of the meshed network. This analysis aims to pinpoint sensitive areas that require enhanced monitoring and control.

The study analyzes loop flow within this system and determines when it occurs. Using the modified Dijkstra algorithm, a path is identified that passes through the line connecting buses 360 and 325, a path that traditional methods, such as the shortest impedance method [6], would not detect. After identifying the branch with the highest sensitivity and the loop flow path it forms, highlighted in red in Fig. 28, the study examines the moment of flow reversal in this line, which occurs after 5.2 p.u., when the power flow crosses zero and reverses direction, as shown in Fig. 27. In Fig. 27, the purple arrow represents the HVDC link, illustrating the direction and magnitude of HVDC power transmission during the analysis. Monitoring these highly sensitive lines is crucial because

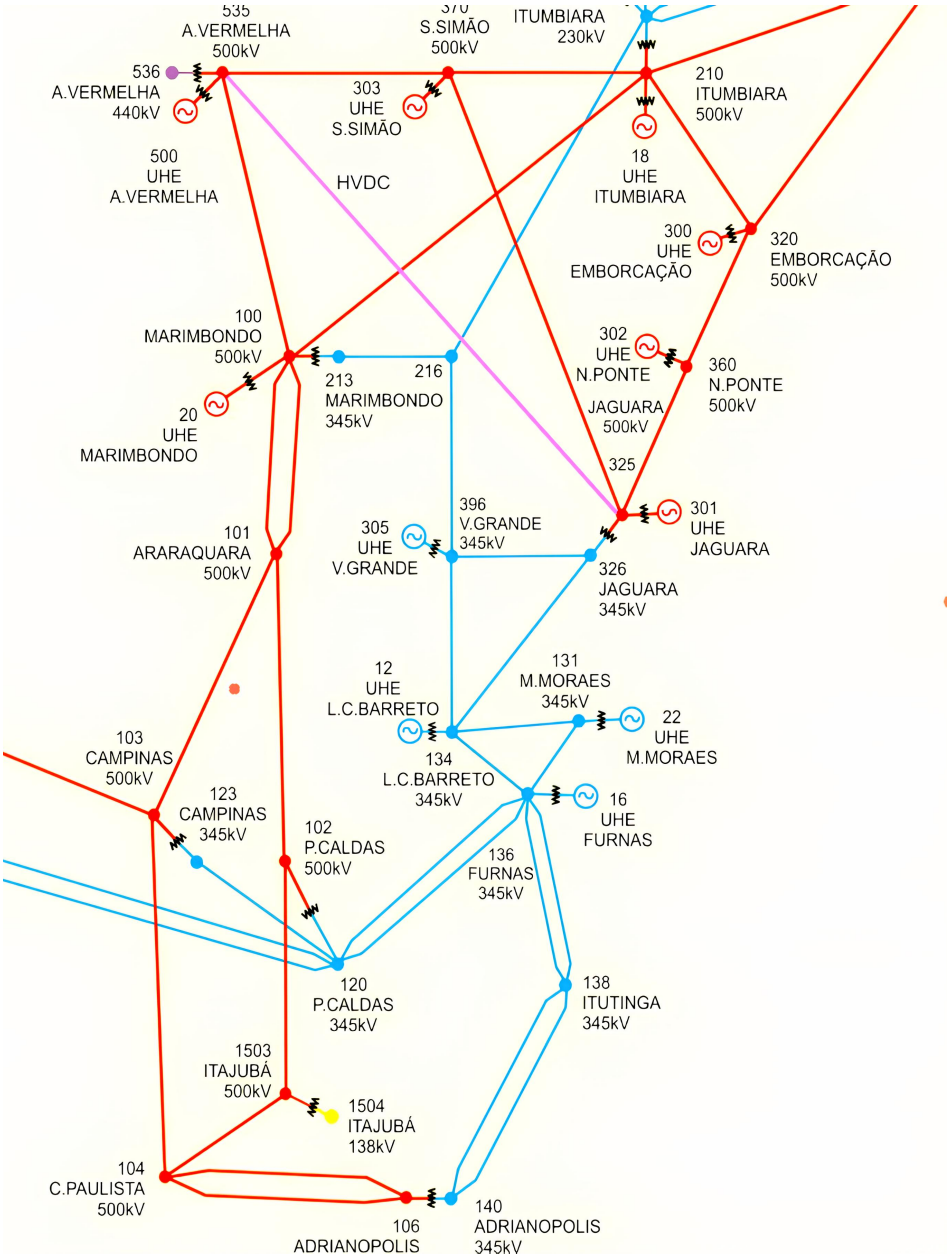

Figure 26: Detail of the Brazilian 107-Bus Test System with embedded HVDC.

they are significantly affected by HVDC power transmission variations, depending on load and generation conditions.

The 107-Bus test system provides a robust framework for examining these phenomena, offering insights into the complexities of managing a

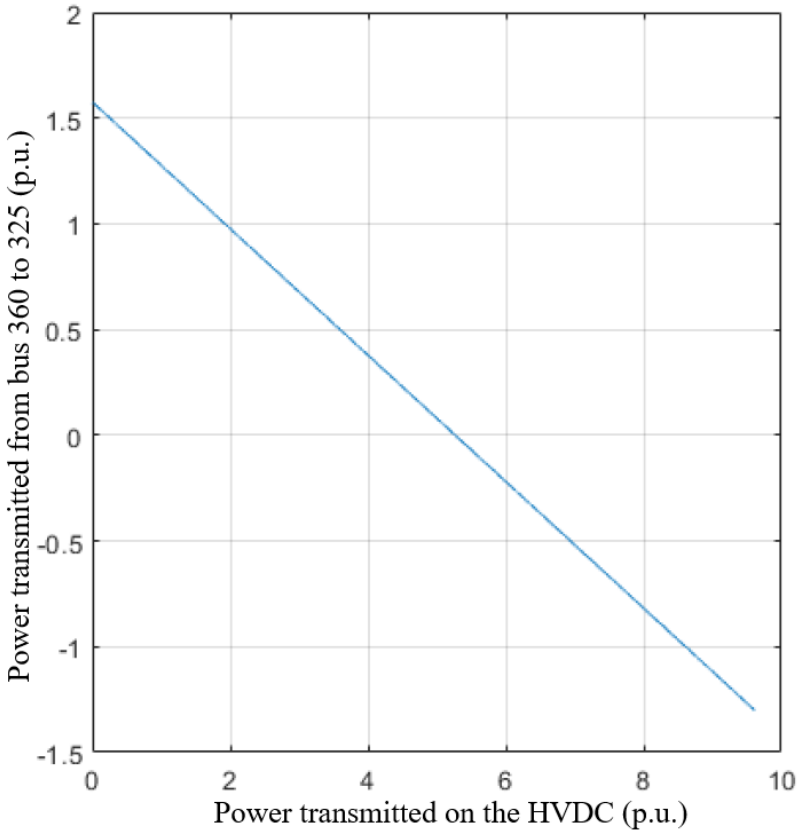

Figure 27: Active Power Flow Between Buses 360 and 325 During HVDC Power Variation.

meshed transmission network with significant renewable generation and load variations. The integration of the HVDC link and the modified Dijkstra algorithm highlights critical areas for system stability and operational efficiency, emphasizing paths that are most affected by loop flows and thus prioritizing resources for effective power flow management.

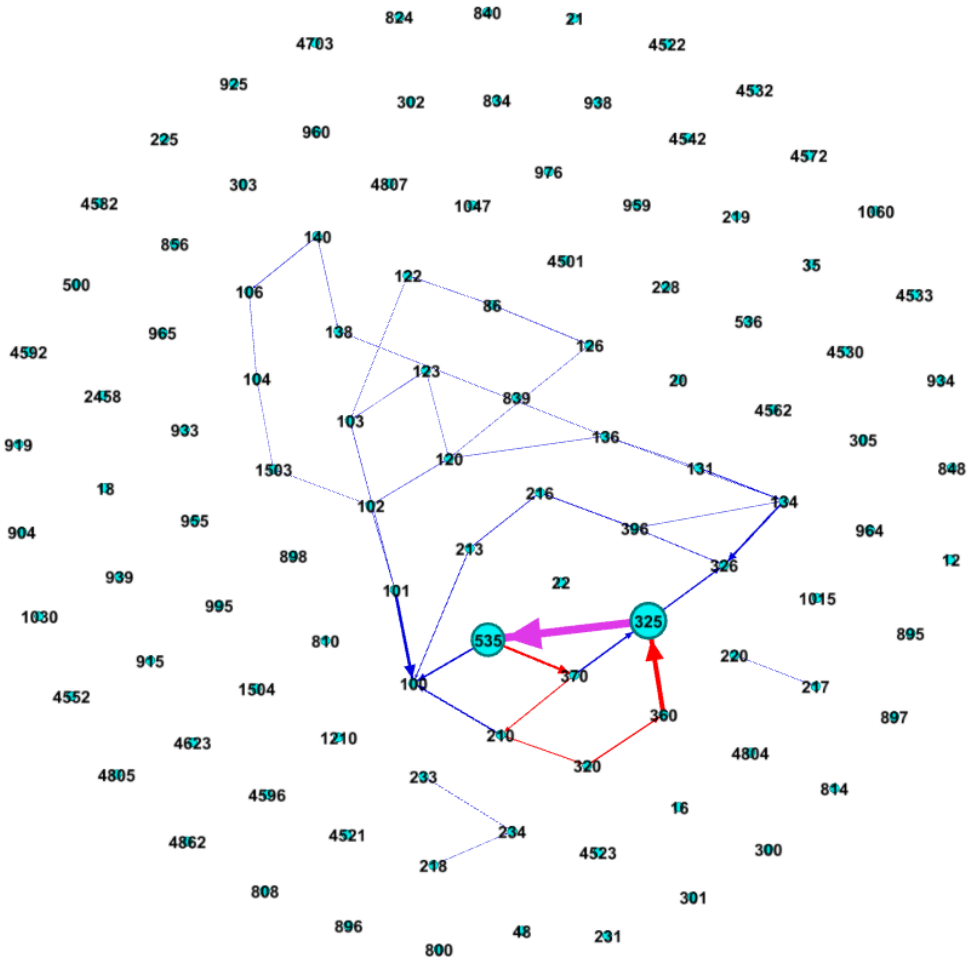

Figure 28: Sensitivity graph of the 107-Bus Brazilian test system.

5 Loss Minimization Framework

This chapter details the optimization formulation aimed at minimizing transmission losses through the embedded HVDC link. This formulation is essential to improving the efficiency of HVDC systems, particularly in the context of long-distance and high-capacity power transmission applications, such as those being implemented in the Brazilian electrical system. For a detailed discussion on HVDC losses, refer to Chapter 4.1.

Let the power generated by the i-th generator of the system be denoted by PG_i. The total real power generated can be modeled as follows:

$$PG_i = PG_{i0} + \Delta PG_i \tag{8}$$

Where PG_{i0} is the base generation and ΔPG_i represents the variation in generation.

The objective function is to minimize the total losses in the system. This can be expressed as:

$$\text{Minimize: } L_{total} = L_{AC} + L_{HVDC} \tag{9}$$

The constraints of the optimization problem include the power balance equation, which is defined as:

$$\begin{aligned} V_k e^{-j\theta_k} \sum_m V_m e^{j\theta_m}(G_{km} + jB_{km}) - V_k^2 G_{km} + \\ V_k V_m G_{km}\cos\theta_{km} + V_k V_m B_{km}\sin\theta_{km} + \\ jV_k^2 B_{km} - jV_k V_m B_{km}\cos\theta_{km} + \\ jV_k V_m G_{km}\sin\theta_{km} - S_{HVDC} = 0 \qquad \forall\ k \end{aligned} \tag{10}$$

Figure 29 illustrates the power balance at Bus k.

The optimization constraints for the system include the limits on the HVDC power flow and the power generated:

$$\underline{P_{HVDC}} \leq P_{HVDC} \leq \overline{P_{HVDC}} \tag{11}$$

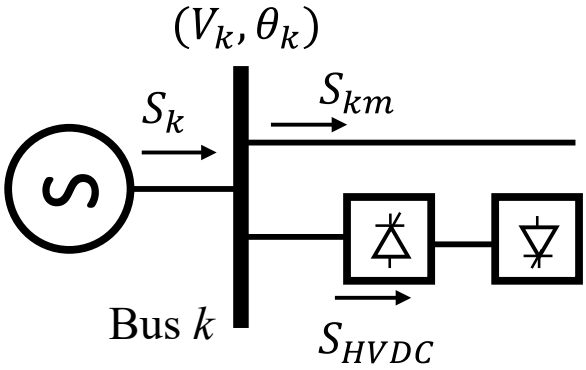

Figure 29: Power balance on Bus k.

$$\underline{PG_k} \leq PG_k \leq \overline{PG_k} \tag{12}$$

Additionally, the voltage magnitude at each bus must be within specified limits:

$$\underline{V_k} \leq V_k \leq \overline{V_k} \tag{13}$$

This formulation provides a framework for optimizing power transmission by minimizing losses and ensuring system reliability and efficiency.

5.1 Proposed Methodology

This study examines the power system's response to two critical factors: topological variations and load changes. The methodology focuses on the role of HVDC control in minimizing system losses by dynamically optimizing power flows. By analyzing the impact of transmission network reconfigurations and varying demand levels, the approach evaluates HVDC's effectiveness in reducing losses and improving system efficiency under different operating conditions.

To clearly present the optimization process, a pseudocode representation is provided in Algorithm 3. While the simulations were conducted using MATLAB, the use of pseudocode enhances clarity and ensures the

methodology is easily understood and reproducible by a broader audience, regardless of the specific programming environment used.

Algorithm 3: HVDC Optimization for Loss Minimization

Input : Power system data (Bus, generation, load, topology)
Output: Optimized HVDC power transfer minimizing system losses

Function `HVDCOptimization(`*System Data*`)`
- Initialize $P_{hvdc} = 0$, $min\_loss = \infty$, $P_{hvdc\_opt} = 0$
- Define constraints (max P_{hvdc}, step size)
- Run initial AC power flow analysis and compute losses
- **for** *step* $= 1$ *to max_steps* **do**
  - Redistribute power from renewable to dispatchable generators in steps of *step_size*
  - **for** $P_{hvdc} = 0$ *to* max_P_h *in increments of step_size* **do**
    - Set HVDC injections: $P_g(source) = P_{hvdc}$, $P_g(target) = -P_{hvdc}$
    - Run AC power flow and compute losses
    - **if** $losses < min\_loss$ **then**
      - Update min_loss, P_{hvdc_opt}
    - **end**
  - **end**
- **end**
- Apply optimized P_{hvdc_opt} and evaluate final losses
- **return** *Optimized HVDC settings and loss reduction*

5.2 Case Studies on HVDC Controlled Power Flow

This chapter presents the simulations and case studies conducted to analyze the effects of HVDC control optimization under varying loading and topological conditions. The analysis focuses on two test systems: the IEEE 57-Bus system and the Brazilian 107-Bus system. The primary objective is to investigate the impact of HVDC control on reducing system losses, particularly in scenarios involving the integration of renewable energy energy and network reconfigurations.

To replicate the real-world effects observed in the Brazilian power system during the 2018 event, where a reduction in wind power generation led to unintended loop flows in the transmission network specific generators were designated as renewable energy sources in these simulations. The study implements a renewable energy case by redistributing power

generation between distant buses to simulate the effect of declining wind generation in one region while increasing dispatchable hydroelectric generation elsewhere to maintain system balance.

In this scenario, power generation is progressively reduced at a selected bus, representing a wind power plant, while a corresponding increase occurs at another bus, representing a hydroelectric plant capable of compensating for the shortfall. A total power redistribution of 2 pu is applied in 40 controlled steps of 0.05 pu, allowing a gradual and systematic assessment of system behavior under dynamic conditions. This approach provides insights into how HVDC control can mitigate the adverse effects of renewable generation fluctuations and prevent loop flow issues.

5.2.1 Application to the IEEE 57-Bus Test Network

The IEEE 57-Bus system is the first test case used to evaluate the effectiveness of HVDC optimization in reducing power losses under varying operating conditions [43]. This system, with its well-structured and moderately complex network, provides an ideal starting point for validating the proposed methodology before applying it to larger, more intricate systems.

By first analyzing the IEEE 57-Bus system, this study establishes a controlled baseline to assess how HVDC control influences system performance. An HVDC link is introduced between Buses 3 and 8, as illustrated in Figure 30, strategically positioned to optimize power transfer and minimize losses. Compared to the previous study in Chapter 3.4.3, the HVDC link location has been modified to highlight the effect of generation redistribution on system performance. The findings from this case study will later be compared with the results from the Brazilian 107-Bus system, ensuring that the insights gained are applicable to networks of different scales and complexities.

The analysis focuses on variations in topology and load conditions to quantify the impact of HVDC control on system losses. The objective is to demonstrate the robustness of the proposed approach and its ability to

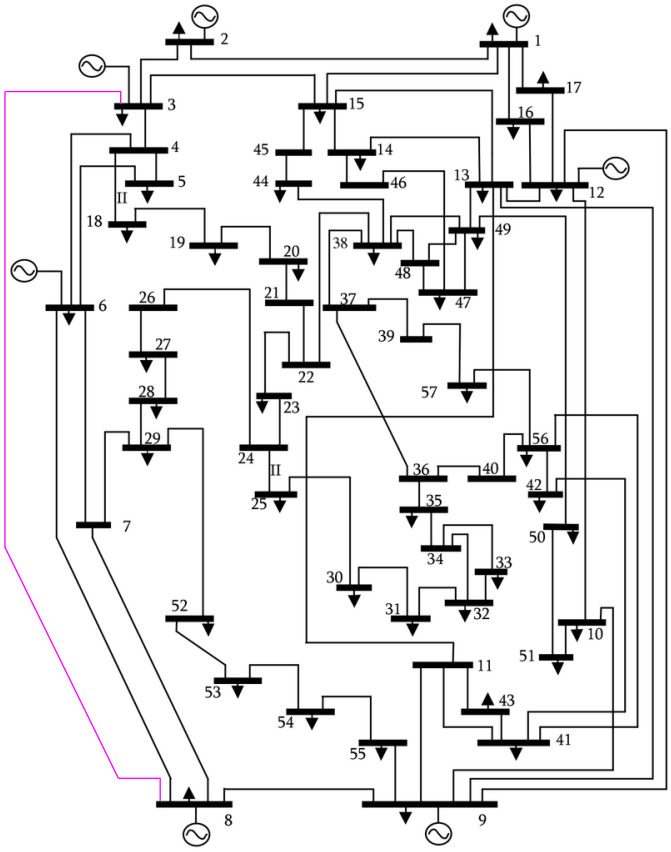

Figure 30: IEEE 57-Bus test system with an embedded HVDC link.

enhance system efficiency in a smaller network with fewer redundancies.

5.2.2 HVDC Response to Different Demand Scenarios

To assess the adaptive capabilities of HVDC control under varying demand, load profiles within the IEEE 57-Bus system were modified. Specifically, three cases were examined: Case 1 (low load, 0.8 pu), Case 2 (moderate load, 0.9 pu), and Case 3 (nominal load, 1.0 pu). These scenarios allowed for the evaluation of HVDC control's impact on system losses across different operating conditions. A simulated power redistribution between Buses 2 and 9, representing a decrease in renewable generation at Bus 2 and a corresponding increase in dispatchable generation at Bus 9, was used to analyze the HVDC system's dynamic balancing

performance.

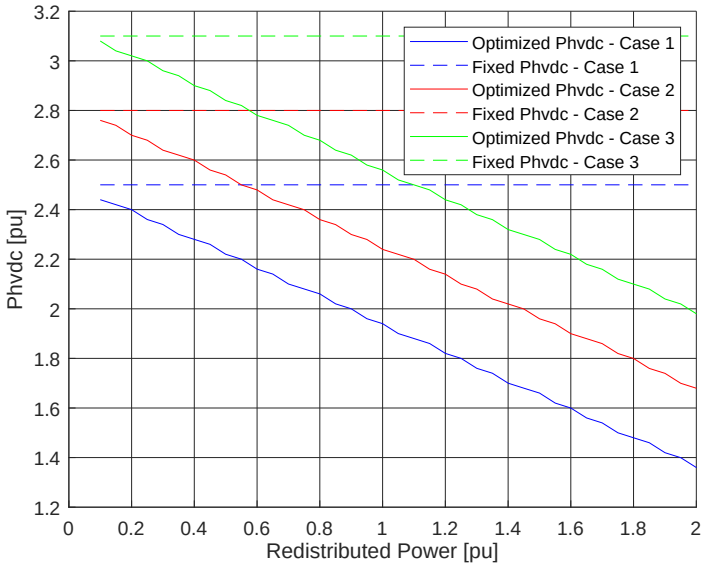

Figure 31: HVDC link power transmission variation across different load conditions.

Figure 31 illustrates the power variation in the HVDC link across the three load scenarios. It highlights how HVDC optimization adjusts power flow to reduce losses and improve operational efficiency compared to cases without HVDC control.

Figure 32 presents the difference in system losses across the load cases. The results show that the loss reduction effect becomes more pronounced as the event progresses. In Case 1 (low load), the initial loss difference is 0.176 pu, increasing to 0.204 pu. Without HVDC optimization, losses would be 15.9% higher, reinforcing the importance of optimized HVDC operation in enhancing efficiency.

5.2.3 HVDC Performance Under Structural Grid Modifications

Using the IEEE 57-Bus system as a model, two case studies were established to analyze the impact of topological changes on HVDC control. In Case 01, the system's response to the opening of the line connecting Buses 22 and 38 is investigated. This analysis, along with Case 02, which focuses on the opening of the line between Buses 38 and 48, examines

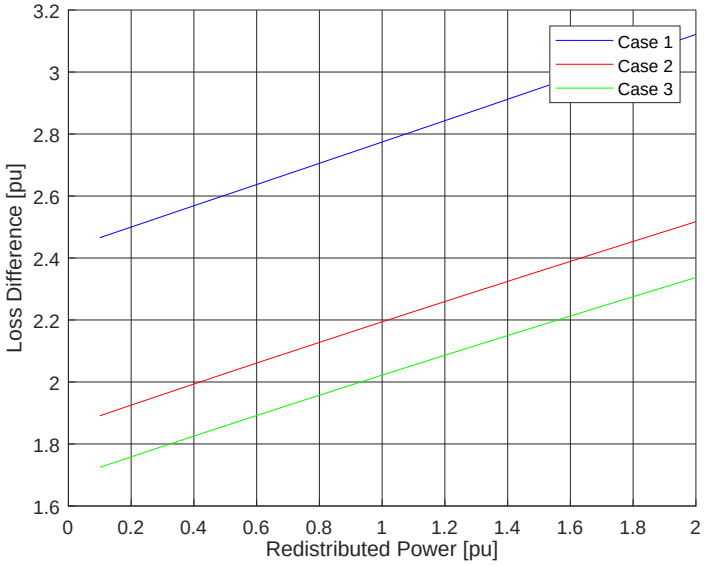

Figure 32: System loss differences with HVDC optimization under different load conditions.

how HVDC control adapts to different network configurations. The selection of these lines is justified by their location in areas of high system sensitivity, as identified in the base configuration. By evaluating power redistribution under these line-opening scenarios, this study quantifies HVDC control's effectiveness in mitigating adverse effects and optimizing power flow to minimize losses. The results demonstrate HVDC's crucial role in maintaining grid stability and optimizing power transfer despite network modifications.

Figure 33 shows the HVDC link power transmission response to different line opening cases, highlighting its adaptability in redirecting power flows.

Figure 34 illustrates the differences in system losses for different topological configurations. When the transmission line between Busses 38 and 48 is open, the loss difference initially measured at 1.72 pu increases to 2.33 pu. Without HVDC control, system losses rise by 35.75%, demonstrating the effectiveness of HVDC in mitigating inefficiencies caused by network topology changes.

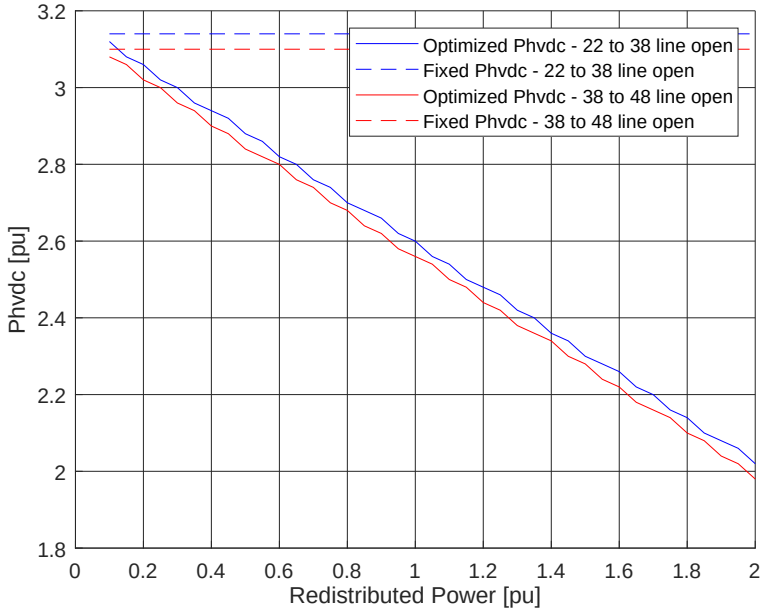

Figure 33: HVDC power transmission variation for different line opening scenarios.

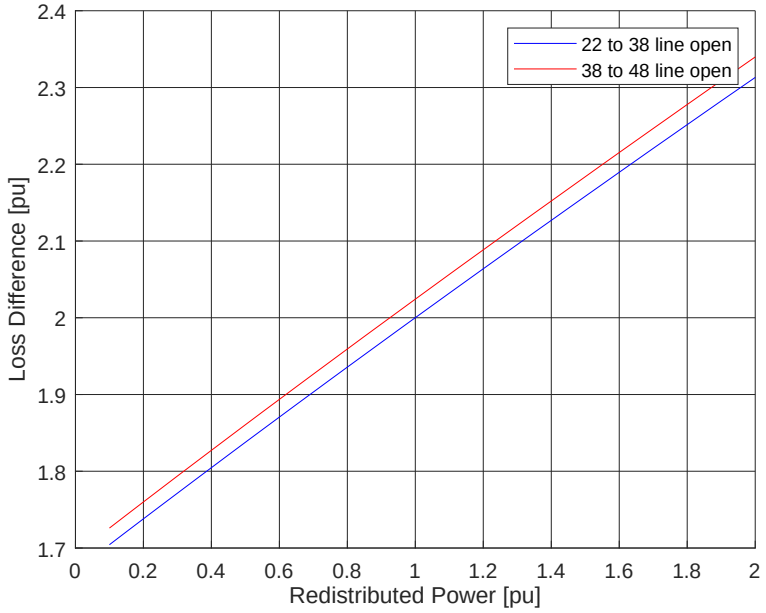

Figure 34: System loss differences with HVDC optimization under various line opening cases.

5.2.4 HVDC Optimization in the Brazilian 107-Bus Network

The second system used in this study is the Brazilian 107-Bus system, which represents the South-Southeast and Mato Grosso regions. This system is utilized to evaluate the interaction between renewable energy sources, such as wind farms, and HVDC control optimization. Two scenarios are analyzed: load variation and topology variation.

Although the actual Brazilian power system in this region does not currently feature significant wind generation or HVDC links, these elements are introduced in the simulation to assess their potential impact on system performance. The study incorporates wind power generation to replicate renewable energy integration challenges and includes an HVDC link to explore its capability in mitigating transmission issues.

An HVDC link is introduced between Buses 325 and 535, highlighted in purple in Figure 26. These buses are strategically selected based on their locations and connectivity to generation sources, enabling a detailed sensitivity analysis of HVDC power transmission in both directions.

The analysis focuses on how variations in topology and load conditions influence system losses, comparing scenarios with and without HVDC optimization. The objective is to assess the potential of HVDC technology to minimize power losses and enhance system efficiency under different operating conditions.

5.2.5 Impact of Load Conditions on HVDC Loss Minimization

This study evaluates the impact of HVDC optimization on system losses under varying load conditions by modifying the load profiles of the Brazilian system. Three distinct cases are considered: Case 1 represents low load conditions (0.7 pu), Case 2 reflects moderate load conditions (0.85 pu), and Case 3 corresponds to nominal load conditions (1 pu). The analysis examines how HVDC control adapts to these cases, mitigating losses and improving system performance under different operational stresses. By comparing results across these load profiles, the study provides insights into the effectiveness of HVDC optimization in enhancing

grid resilience and efficiency under diverse demand conditions.

The power redistribution event was carried out between Buses 303 and 16, simulating the effect of a drop in renewable generation at Bus 303 and compensation by Bus 16 with dispatchable generation. This scenario allows for analyzing how HVDC control responds to an unexpected reduction in renewable power injection and its ability to balance power flows efficiently.

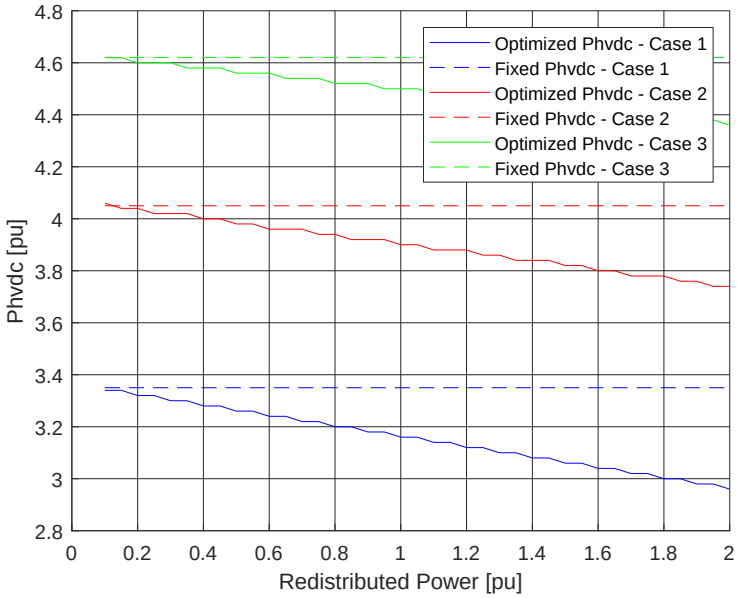

Figure 35: Variation of transmitted power in the HVDC link, diferent loads cases.

Figure 35 illustrates the difference in power transmission through the HVDC link when HVDC control is applied to minimize system losses, compared to the scenario where control is not applied. This comparison highlights the adaptive response of HVDC control in redistributing power flow to improve overall system efficiency.

Figure 36 presents the difference in system losses across the three load cases. The loss difference increases throughout the event since the comparison is made between cases with and without HVDC control. Without HVDC optimization, power distribution is less efficient, leading to higher losses as the event progresses. The results demonstrate the effectiveness

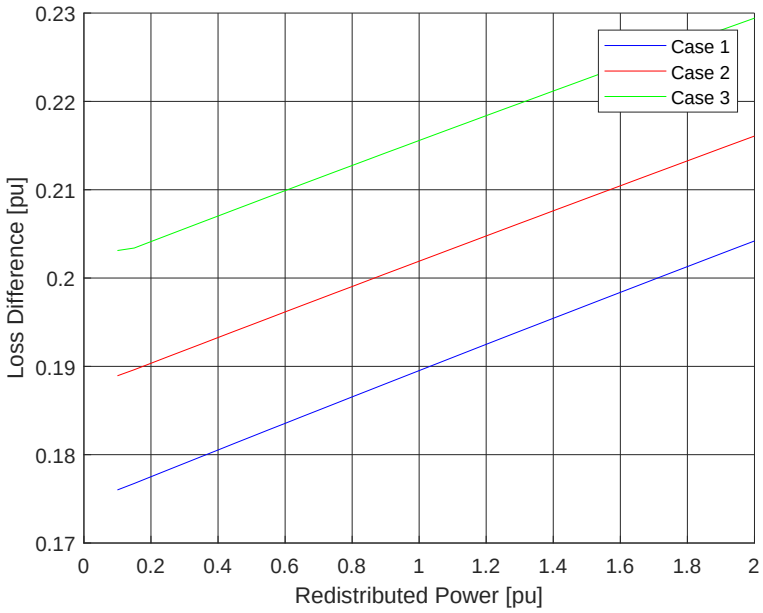

Figure 36: Difference in system losses using HVDC optimization.

of HVDC in dynamically adjusting power flows to minimize system losses under varying demand conditions.

In Case 3, which represents the nominal system power condition, the initial loss difference is 0.203 pu, increasing to 0.229 pu by the end of the event. Without HVDC control, losses would be 12.8% higher, highlighting the significant impact of optimized HVDC operation in improving system efficiency.

5.2.6 Impact of Grid Reconfiguration on HVDC Power Transfer

This analysis examines the impact of different transmission network configurations by simulating the opening and closing of specific transmission lines. It evaluates how HVDC control adapts to these changes and optimizes system losses. The objective is to assess the role of HVDC in maintaining efficiency under varying topological conditions.

The study analyzes power redistribution under various line opening scenarios to determine HVDC control's effectiveness in mitigating adverse effects. By adjusting power flows, HVDC redistributes loads effi-

ciently and maintains system stability despite network reconfigurations.

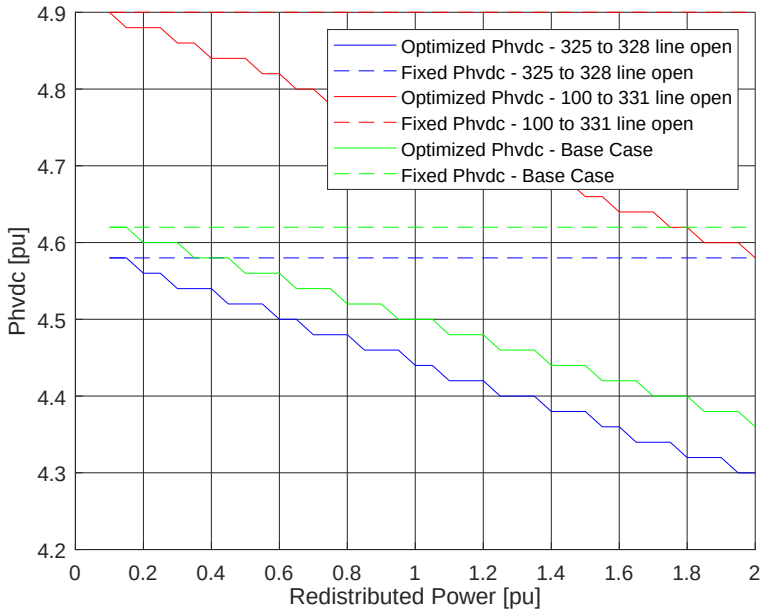

Figure 37: Transmitted power variation in the HVDC link for different line opening cases.

Figure 37 shows the variation in HVDC power transmission under different transmission line opening scenarios. The figure exhibits a staircase-like pattern, which reflects the step-by-step nature of the HVDC control strategy. At each step, the system losses is evaluated, and the transmitted power through the HVDC link is recalculated based on the updated network conditions. This iterative adjustment allows the HVDC link to dynamically compensate for topological changes, mitigating the impact of transmission constraints and improving overall system performance.

Figure 38 presents system loss differences across different topological configurations. As transmission lines open, losses increase due to power flow redistribution. HVDC optimization significantly mitigates these losses, demonstrating its role in preserving system efficiency and reducing power dissipation.

In the most critical scenario, where a major transmission corridor opens, the initial loss difference is 0.208 pu, increasing to 0.237 pu. Without HVDC control, losses rise by 13.94%, underscoring HVDC's role in improving grid resilience and optimizing power distribution under vary-

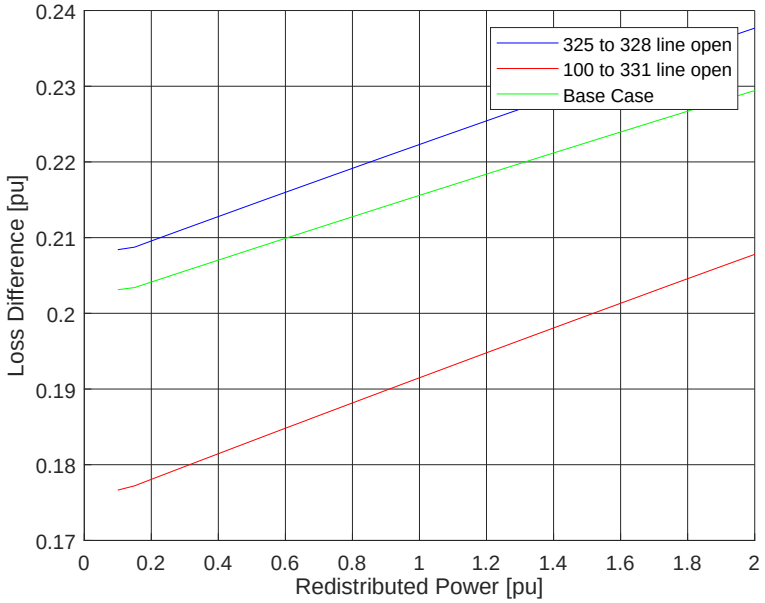

Figure 38: System loss differences with HVDC optimization across various line opening cases.

ing transmission conditions.

5.3 Publications Derived from This Thesis

The research conducted in this Ph.D. Thesis has led to the following scientific publications:

- **Published:** *Analysis of Loop Flow in Electrical Power Systems with Embedded HVDC Using a Modified Dijkstra Algorithm*, Sustainable Energy, Grids & Networks, 2025. [DOI: 10.1016/j.segan.2024.101597]
- **To be submitted:** *Mitigating Loop Flow, Minimizing Power Losses in HVDC Systems.*

These publications contribute to the academic and professional community by providing new methodologies for analyzing and optimizing power flow in systems with embedded HVDC links. The findings presented support further research on transmission efficiency, loop flow mitigation, and loss optimization in modern power grids.

6 Conclusion

This Ph.D. Thesis has presented a comprehensive analysis of loop flow scenarios in power systems with embedded HVDC links and proposed methodologies for their identification, mitigation, and optimization. The research was structured into two main studies: the first focusing on the identification and analysis of loop flow paths using a modified Dijkstra algorithm, and the second on optimizing power losses in AC transmission systems by leveraging HVDC injections as control variables.

The first study introduced a novel approach for identifying key paths within a loop system, allowing for the detection of potential loop flows. By applying a sensitivity analysis, this method effectively pinpointed the most critical branches within the system and assessed their influence on power flow variations. One of the key findings of this research was the identification of an optimal loss minimization point, beyond which losses begin to increase again, signaling the onset of loop flow. The ability to predict such scenarios provides system operators with a powerful tool for improving operational planning and mitigating adverse effects caused by uncontrolled power redistribution.

Building upon these insights, the second study developed an optimization framework aimed at minimizing AC system losses through HVDC power injections. By treating these injections as control variables, the methodology effectively reduced transmission losses while indirectly mitigating loop flow effects. Since loss minimization follows a parabolic trend, with its lowest point corresponding to the threshold before significant loop flows emerge, the study demonstrated that explicitly incorporating loop flow constraints would be redundant. Instead, the proposed optimization approach inherently addresses the issue, offering a practical and computationally efficient method for system operators.

The proposed methodologies have significant implications for the operation and planning of modern power systems. The modified Dijkstra algorithm provides a systematic way to analyze loop flow paths and identify potential weak points in the system, enabling operators to anticipate

and respond to changes in power flow direction. Additionally, the HVDC loss optimization framework enhances system efficiency, particularly in scenarios with high renewable energy penetration and dynamic loading conditions.

Despite its advantages, the approach has certain limitations. While it effectively captures the primary factors influencing loop flow and loss optimization, it does not explicitly account for transient stability constraints, long-term thermal limits, or complex HVDC control dynamics. Future research could integrate these aspects into the framework to develop a more holistic system assessment. Moreover, the methodology primarily focuses on steady-state analysis, and incorporating dynamic system responses could further enhance its applicability. Considering multi-HVDC embedded systems to evaluate methods for detecting and mitigating loop flows and optimizing losses is yet to be explored.

Overall, this Ph.D. Thesis contributes to the field of power system optimization by providing innovative methodologies for loop flow identification and loss minimization in HVDC-integrated networks. The insights gained from this work support the development of more resilient, efficient, and adaptive transmission systems, paving the way for enhanced grid stability and reliability in the face of evolving energy landscapes and increasing renewable energy integration.

References

[1] EPE - Brazilian Transmission System Planning Company, *Website:* www.epe.gov.br/en.

[2] Rafael O. Fernandes and Maria C.D. Tavares, *Mitigation of the commutation failure problem in the HVDC multi-infeed scenario in Brazil using synchronized phasor measurement*, Electric Power Systems Research, vol. 235, pp. 110829, 2024, doi:10.1016/j.epsr.2024.110829.

[3] Glauco N. Taranto, Carlos E.V. Pontes, Thomas M. Campello, Victor A.F. Almeida, John Graham, Paulo C.V. Esmeraldo, and Ma Schicong, *Power flow control for an embedded HVDC link to integrate renewable energy in Brazil*, Electric Power Systems Research, vol. 211, pp. 108504, 2022, doi:10.1016/j.epsr.2022.108504.

[4] Mokhtar Benasla, Tayeb Allaoui, Mostefa Brahami, Vijay K. Sood, and Mouloud Denaï, *Power system security enhancement by HVDC links using a closed-loop emergency control*, Electric Power Systems Research, vol. 168, pp. 228-238, 2019, doi:10.1016/j.epsr.2018.12.002.

[5] L. Zanella, B.A.S. Ambrósio, G.R. Moraes, I.C. Decker, A.F.C. Aquino, and D. Issicaba, *Design of a machine learning model to enhance the arming of the system integrity protection scheme of the Brazilian North-Southeast HVDC Bipoles*, Electric Power Systems Research, vol. 235, pp. 110647, 2024, doi:10.1016/j.epsr.2024.110647.

[6] Manish Mohanpurkar, Daniel Zimmerle, and Siddharth Suryanarayanan, *An algorithmic approach to tracing closed loops in a power systems network*, 2015 North American Power Symposium (NAPS), 2015, pp. 1-6, doi:10.1109/NAPS.2015.7335178.

[7] Tang Zhong, *Graph theory based expert system to form de-icing route in Changsha power grid*, International Journal of Electrical Power & Energy Systems, vol. 43, no. 1, pp. 1318-1321, 2012, doi:10.1016/j.ijepes.2012.03.044.

[8] V.S.C. Lim, J.D.F. McDonald, and T.K. Saha, *Application of loop frame of reference to power flow tracing and loss allocation*, 2005 International Power Engineering Conference, 2005, pp. 1013-1018 Vol. 2, doi:10.1109/IPEC.2005.207056.

[9] K. Iba, *Identification of transmission line user and congestion management by loop flow controllers*, International Symposium CIGRE/IEEE PES, 2005, pp. 307-314, doi:10.1109/CIGRE.2005.1532756.

[10] Felipe Arraño-Vargas and Georgios Konstantinou, *Longitudinal power systems for modern and future grid studies: A graph theory analysis*, Sustainable Energy, Grids and Networks, vol. 35, pp. 101132, 2023, doi:10.1016/j.segan.2023.101132.

[11] K. Karoui, C. Rahmann, and A. Arriagada, *AC interconnection between longitudinal power systems - The Chilean case*, 2015 IEEE Power & Energy Society General Meeting, pp. 1-6, 2015, doi:10.1109/PESGM.2015.7286648.

[12] Wei Wu and Chikong Wong, *FACTS applications in preventing loop flows in interconnected systems*, 2003 IEEE Power Engineering Society General Meeting (IEEE Cat. No.03CH37491), 2003, pp. 170-174 Vol. 1, doi:10.1109/PES.2003.1267161.

[13] Katharina Frey, Pascal Wiest, Krzysztof Rudion, and Jochen Christian, *Automated operation of parallel VSC HVDC links within an interconnected AC network*, 2016 IEEE Power and Energy Society General Meeting (PESGM), 2016, pp. 1-5.

[14] Z. Li, R. Zhan, Y. Li, Y. He, J. Hou, X. Zhao, and X.-P. Zhang, *Recent developments in HVDC transmission systems to support renewable energy integration*, Global Energy Interconnection, vol. 1, no. 5, pp. 595-607, 2018, doi:10.14171/j.2096-5117.gei.2018.05.009.

[15] B. R. T. Cotts, J. R. Prigmore, and K. L. Graf, *HVDC Transmission for Renewable Energy Integration*, in The Power Grid, B. W. D'Andrade, Ed. Academic Press, 2017, pp. 171-196, doi:10.1016/B978-0-12-805321-8.00006-9.

[16] J. Lee, S. Park, and J.-K. Park, *Development of a Loss Minimization Based Operation Strategy for Embedded BTB VSC HVDC*, Applied Sciences, vol. 9, no. 11, pp. 2234, 2019, doi:10.3390/app9112234.

[17] Rakibuzzaman Shah, Jesus C. Sánchez, Robin Preece, and Mike Barnes, *Stability and control of mixed AC–DC systems with VSC-*

HVDC: a review, IET Generation, Transmission & Distribution, vol. 12, no. 10, pp. 2207-2219, 2018, doi:10.1049/iet-gtd.2017.1140.

[18] P. A. Gbadega and Y. Sun, *Synergistic Integration of Renewable Energy and HVDC Technology for Enhanced Multi-objective Economic Emission Dispatch Using the Salp Swarm Algorithm*, in Neural Computing for Advanced Applications, H. Zhang, X. Li, T. Hao, W. Meng, Z. Wu, and Q. He, Eds. Springer Nature Singapore, 2025, pp. 232–249, doi:10.1007/978-981-97-7004-5.

[19] X. Zhao, Y. Zhang, Y. Li, and X.-P. Zhang, *Coordinated Control Strategies of VSC-MTDC for Enhancing Offshore Wind Power Integration*, IEEE Transactions on Power Delivery, vol. 35, no. 2, pp. 576-587, 2020, doi:10.1109/TPWRD.2019.2937194.

[20] J. González-Cabrera, F. Jurado, and A. J. Gil-Mena, *Optimization of hybrid AC/DC networks using power flow shift factors and metaheuristic techniques*, Electric Power Systems Research, vol. 192, pp. 106395, 2021, doi:10.1016/j.epsr.2020.106395.

[21] I. Bakır, M. Uzunoglu, and O. Guler, *Optimal Power Flow for Hybrid AC/DC Power Systems Considering Renewable Energy Sources*, IEEE Transactions on Industry Applications, vol. 58, no. 3, pp. 4036-4045, 2022, doi:10.1109/TIA.2022.3140150.

[22] H. Wang, S. N. Singh, and J. Østergaard, *Impact of AC Line Modeling on Optimal Power Flow with VSC-Based Multi-Terminal DC System*, IEEE Transactions on Power Systems, vol. 28, no. 4, pp. 3894-3904, 2013, doi:10.1109/TPWRS.2013.2273483.

[23] C. Chen, Z. Xu, and Y. Zhang, *An Optimal Power Flow Model Considering VSC-HVDC and Renewable Energy Fluctuations*, IEEE Access, vol. 10, pp. 35440-35449, 2022, doi:10.1109/ACCESS.2022.3164136.

[24] T.M. Campello, F.N.F. Dicler, S.L. Varricchio, H.M. de Barros, C.O. Costa, A.C.S. Lima, and G.N. Taranto, *Reviewing the large electrical*

network equivalent methods under development for electromagnetic transient studies in the Brazilian Interconnected power system, International Journal of Electrical Power & Energy Systems, vol. 151, pp. 109033, 2023, doi:10.1016/j.ijepes.2023.109033.

[25] R. Zymler, A. M. Silva, et al, *Operation Planning of the North-Southeast Interconnection with the Xingu-Estreito and Xingu-Terminal Rio HVDC Links*, XXV SNPTEE, Belo Horizonte, 2019.

[26] Fabio A. Diuana, Cindy Viviescas, and Roberto Schaeffer, *An analysis of the impacts of wind power penetration in the power system of southern Brazil*, Energy, vol. 186, pp. 115869, 2019, doi:10.1016/j.energy.2019.115869.

[27] de A. Pedroso, Felipe R. V., Bassini, Marcos T., Horita, Marco A. B., Jardini, Jose A., Graham, John F., Liu, Guijun. HVDC multi-infeed analysis of the Brazilian transmission system and possible mitigation methods. *CSEE Journal of Power and Energy Systems*, 2018, 4(4): 487-494. doi: 10.17775/CSEEJPES.2016.01700.

[28] Prado, Fernando Amaral de Almeida. Chapter 17 - How much is possible? An integrative study of intermittent and renewables sources deployment. A case study in Brazil. In: Ren, Jingzheng, ed. *Renewable-Energy-Driven Future*. Academic Press, 2021, pp. 511-538. doi: 10.1016/B978-0-12-820539-6.00017-0.

[29] Rosas, Gracita Batista, Lourenço, Elizete Maria, Falcão, Djalma Mosqueira, Fernandes, Thelma Solange Piazza. An Expeditious Methodology to Assess the Effects of Intermittent Generation on Power Systems. *Energies*, 2019, 12(6): 1135. doi: 10.3390/en12061135.

[30] Lap, Tjerk, Benders, René, van der Hilst, Floor, Faaij, André. How does the interplay between resource availability, intersectoral competition and reliability affect a low-carbon power generation mix in Brazil for 2050? *Energy*, 2020, 195: 116948. doi: 10.1016/j.energy.2020.116948.

[31] Melo, Ranther, Torres, Carlos, Borba, Bruno, Dias, Bruno. Multi-year two-stage generation and transmission expansion planning: intermittent renewable energy sources integration for Brazilian interconnected power system. *Electrical Engineering*, 2022, 104(4): 2689-2701. doi: 10.1007/s00202-021-01456-6.

[32] ONS - Brazilian National System Operator, Energy Now - Load and Generation, *Website:* www.ons.org.br/paginas/energia-agora/carga-e-geracao.

[33] National Electric System Operator (ONS), *Maps for download*, https://www.ons.org.br/paginas/sobre-o-sin/mapas, visited on May 5, 2023.

[34] H. Jiang and A. Ekstrom, *Multiterminal HVDC systems in urban areas of large cities*, IEEE Transactions on Power Delivery, vol. 13, no. 4, pp. 1278-1284, 1998, doi:10.1109/61.714496.

[35] J. Liang, O. Gomis-Bellmunt, J. Ekanayake, and N. Jenkins, *Control of multi-terminal VSC-HVDC transmission for offshore wind power*, in *Proc. 13th Eur. Conf. Power Electron. Appl.*, 2009, pp. 1-10.

[36] H. Dong, Z. Xu, P. Song, G. Tang, Q. Xu, and L. Sun, *Optimized power redistribution of offshore wind farms integrated VSC-MTDC transmissions after onshore converter outage*, IEEE Transactions on Industrial Electronics, vol. 64, no. 11, pp. 8948-8958, 2017, doi:10.1109/TIE.2016.2631136.

[37] D. Yang, K. Zhao, and Y. Liu, *Coordinated optimization for controlling short circuit current and multi-infeed DC interaction*, Journal of Modern Power Systems and Clean Energy, vol. 2, no. 1, pp. 374–384, 2014, doi:10.1007/s40565-014-0081-z.

[38] Wang Shu-Xi, *The Improved Dijkstra's Shortest Path Algorithm and Its Application*, Procedia Engineering, vol. 29, pp. 1186-1190, 2012, doi:10.1016/j.proeng.2012.01.110.

[39] Shaoyan Li, Zimian Lin, Youhao Zhang, Xueping Gu, and Hongtao Wang, *Optimization method of skeleton network partitioning scheme considering resilience active improvement in power system restoration after typhoon passes through*, International Journal of Electrical Power & Energy Systems, vol. 148, pp. 109001, 2023, doi:10.1016/j.ijepes.2023.109001.

[40] Saleh Aghajan-Eshkevari, Mohammad Taghi Ameli, and Sasan Azad, *Optimal routing and power management of electric vehicles in coupled power distribution and transportation systems*, Applied Energy, vol. 341, pp. 121126, 2023, doi:10.1016/j.apenergy.2023.121126.

[41] Ghaffar Yousefi, Aleksandar Dimovski, Lucio Radaelli, and Marco Merlo, *Estimating the impact of electric mobility on distribution networks through GIS techniques*, Sustainable Energy, Grids and Networks, vol. 38, pp. 101379, 2024, doi:10.1016/j.segan.2024.101379.

[42] Gogulamudi Pradeep Reddy, Yellapragada Venkata Pavan Kumar, Maddikera Kalyan Chakravarthi, and Aymen Flah, *Refined Network Topology for Improved Reliability and Enhanced Dijkstra Algorithm for Optimal Path Selection during Link Failures in Cluster Microgrids*, Sustainability, vol. 14, no. 16, pp. 10367, 2022, doi:10.3390/su141610367.

[43] Robert D. Christie, *Power systems test case archive*, Department of Electrical Engineering, University of Washington, 1993. Available at: https://labs.ece.uw.edu/pstca/

[44] A.C. Zambroni de Souza, Fritz W. Mohn, Isabella F. Borges, and Tito R. Ocariz, *Using PV and QV curves with the meaning of static contingency screening and planning*, Electric Power Systems Research, vol. 81, no. 7, pp. 1491-1498, 2011, doi:10.1016/j.epsr.2011.02.012.

[45] H. Ambriz-Pérez, E. Acha, and C.R. Fuerte-Esquivel, *High voltage direct current modelling in optimal power flows*, International Jour-

nal of Electrical Power & Energy Systems, vol. 30, no. 3, pp. 157-168, 2008, doi:10.1016/j.ijepes.2007.06.010.

[46] Adil Mansouri, Abderazzak Ammar, Abdelmounime El Magri, Nabil Elaadouli, El Khlifi Younes, Rachid Lajouad, and Fouad Giri, *An adaptive control strategy for integration of wind farm using a VSC-HVDC transmission system*, Results in Engineering, vol. 23, pp. 102359, 2024, doi:10.1016/j.rineng.2024.102359.

[47] W. Alves, *Proposição de Sistemas Teste para Análise Computacional de Sistemas de Potência*, Ph.D. thesis, Faculdade de Engenharia, Universidade Federal, 2007.

A Appendix - Test systems data

In this chapter, the data of the test systems is presented.

A.1 IEEE 4 bus adapted

Table 8: IEEE 4 bus adapted data

Number	Tipe	V	A	Pl	Ql	Pg	Qg	Qmax	Qmin
1	3	1.000	0.0	0.0	0.0	0.0	0.0	999.9	-999.9
2	2	0.950	0.0	40.0	12.5	90.0	-16.0	90.0	-20.0
3	0	0.900	0.0	50.0	16.5	0.0	0.0	50.0	-999.9
4	2	0.900	0.0	20.0	12.5	10.0	0.0	30.0	-20.0

Table 9: IEEE 4 bus adapted branch data

From	To	Rpu	Xpu	Tap	Tmn	Tmx	step
1	2	0.0200	0.1000	0.0	0.0	0.0	0.0
2	3	0.1000	0.2000	0.0	0.0	0.0	0.0
3	4	0.1000	0.2000	1.0	0.8	1.2	0.05

A.2 IEEE 14 bus

Table 10: IEEE 14 bus data

Number	Type	V	A	Pl	Ql	Pg	Qg	Qmax	Qmin
1	3	1.060	0.0	0.0	0.0	232.4	-16.9	0.0	0.0
2	2	1.045	-4.98	21.7	12.7	166.0	42.4	50.0	-40.0
3	2	1.010	-12.72	94.2	19.0	0.0	23.4	40.0	0.0
4	0	1.019	-10.33	47.8	-3.9	0.0	0.0	0.0	0.0
5	0	1.020	-8.78	7.6	1.6	0.0	0.0	0.0	0.0
6	2	1.070	-14.22	11.2	7.5	0.0	12.2	24.0	-6.0
7	0	1.062	-13.37	0.0	0.0	0.0	0.0	0.0	0.0
8	2	1.090	-13.36	0.0	0.0	0.0	17.4	24.0	-6.0
9	0	1.056	-14.94	29.5	16.6	0.0	0.0	0.0	0.0
10	0	1.051	-15.10	9.0	5.8	0.0	0.0	0.0	0.0
11	0	1.057	-14.79	3.5	1.8	0.0	0.0	0.0	0.0
12	0	1.055	-15.07	6.1	1.6	0.0	0.0	0.0	0.0
13	0	1.050	-15.16	13.5	5.8	0.0	0.0	0.0	0.0
14	0	1.036	-16.04	14.9	5.0	0.0	0.0	0.0	0.0

Table 11: IEEE 14 bus branch data

From	To	Rpu	Xpu	Line charging
1	2	0.01938	0.05917	0.0528
1	5	0.05403	0.22304	0.0492
2	3	0.04699	0.19797	0.0438
2	4	0.05811	0.17632	0.0374
2	5	0.05695	0.17388	0.0340
3	4	0.06701	0.17103	0.0346
4	5	0.01335	0.04211	0.0128
4	7	0.0	0.20912	0.0
4	9	0.0	0.55618	0.0

From	To	Rpu	Xpu	Line charging
5	6	0.0	0.25202	0.0
6	11	0.09498	0.19890	0.0
6	12	0.12291	0.25581	0.0
6	13	0.06615	0.13027	0.0
7	8	0.0	0.17615	0.0
7	9	0.0	0.11001	0.0
9	10	0.03181	0.08450	0.0
9	14	0.12711	0.27038	0.0
10	11	0.08205	0.19207	0.0
12	13	0.22092	0.19988	0.0
13	14	0.17093	0.34802	0.0

A.3 IEEE 57 bus

Table 12: IEEE 57 bus data

Number	Type	V	A	Pl	Ql	Pg	Qg	Qmax	Qmin
1	3	1.040	0.0	55.0	17.0	128.9	-16.1	0.0	0.0
2	2	1.010	-1.18	3.0	88.0	0.0	-0.8	50.0	-17.0
3	2	0.985	-5.97	41.0	21.0	40.0	-1.0	60.0	-10.0
4	0	0.981	-7.32	0.0	0.0	0.0	0.0	0.0	0.0
5	0	0.976	-8.52	13.0	4.0	0.0	0.0	0.0	0.0
6	2	0.980	-8.65	75.0	2.0	0.0	0.8	25.0	-8.0
7	0	0.984	-7.58	0.0	0.0	0.0	0.0	0.0	0.0
8	2	1.005	-4.45	150.0	22.0	450.0	62.1	200.0	-140.0
9	2	0.980	-9.56	121.0	26.0	0.0	2.2	9.0	-3.0
10	0	0.986	-11.43	5.0	2.0	0.0	0.0	0.0	0.0
11	0	0.974	-10.17	0.0	0.0	0.0	0.0	0.0	0.0
12	2	1.015	-10.46	377.0	24.0	310.0	128.5	155.0	-150.0
13	0	0.979	-9.79	18.0	2.3	0.0	0.0	0.0	0.0
14	0	0.970	-9.33	10.5	5.3	0.0	0.0	0.0	0.0
15	0	0.988	-7.18	22.0	5.0	0.0	0.0	0.0	0.0
16	0	1.013	-8.85	43.0	3.0	0.0	0.0	0.0	0.0
17	0	1.017	-5.39	42.0	8.0	0.0	0.0	0.0	0.0
18	0	1.001	-11.71	27.2	9.8	0.0	0.0	0.0	0.0
19	0	0.970	-13.20	3.3	0.6	0.0	0.0	0.0	0.0
20	0	0.964	-13.41	2.3	1.0	0.0	0.0	0.0	0.0
21	0	1.008	-12.89	0.0	0.0	0.0	0.0	0.0	0.0
22	0	1.010	-12.84	0.0	0.0	0.0	0.0	0.0	0.0
23	0	1.008	-12.91	6.3	2.1	0.0	0.0	0.0	0.0
24	0	0.999	-13.25	0.0	0.0	0.0	0.0	0.0	0.0
25	0	0.982	-18.13	6.3	3.2	0.0	0.0	0.0	0.0
26	0	0.959	-12.95	0.0	0.0	0.0	0.0	0.0	0.0
27	0	0.982	-11.48	9.3	0.5	0.0	0.0	0.0	0.0

Number	Type	V	A	Pl	Ql	Pg	Qg	Qmax	Qmin
28	0	0.997	-10.45	4.6	2.3	0.0	0.0	0.0	0.0
29	0	1.010	-9.75	17.0	2.6	0.0	0.0	0.0	0.0
30	0	0.962	-18.68	3.6	1.8	0.0	0.0	0.0	0.0
31	0	0.936	-19.34	5.8	2.9	0.0	0.0	0.0	0.0
32	0	0.949	-18.46	1.6	0.8	0.0	0.0	0.0	0.0
33	0	0.947	-18.50	3.8	1.9	0.0	0.0	0.0	0.0
34	0	0.959	-14.10	0.0	0.0	0.0	0.0	0.0	0.0
35	0	0.966	-13.86	6.0	3.0	0.0	0.0	0.0	0.0
36	0	0.976	-13.59	0.0	0.0	0.0	0.0	0.0	0.0
37	0	0.985	-13.41	0.0	0.0	0.0	0.0	0.0	0.0
38	0	1.013	-12.71	14.0	7.0	0.0	0.0	0.0	0.0
39	0	0.983	-13.46	0.0	0.0	0.0	0.0	0.0	0.0
40	0	0.973	-13.62	0.0	0.0	0.0	0.0	0.0	0.0
41	0	0.996	-14.05	6.3	3.0	0.0	0.0	0.0	0.0
42	0	0.966	-15.50	7.1	4.4	0.0	0.0	0.0	0.0
43	0	1.010	-11.33	2.0	1.0	0.0	0.0	0.0	0.0
44	0	1.017	-11.86	12.0	1.8	0.0	0.0	0.0	0.0
45	0	1.036	-9.25	0.0	0.0	0.0	0.0	0.0	0.0
46	0	1.050	-11.89	0.0	0.0	0.0	0.0	0.0	0.0
47	0	1.033	-12.49	29.7	11.6	0.0	0.0	0.0	0.0
48	0	1.027	-12.59	0.0	0.0	0.0	0.0	0.0	0.0
49	0	1.036	-12.92	18.0	8.5	0.0	0.0	0.0	0.0
50	0	1.023	-13.39	21.0	10.5	0.0	0.0	0.0	0.0
51	0	1.052	-12.52	18.0	5.3	0.0	0.0	0.0	0.0
52	0	0.980	-11.47	4.9	2.2	0.0	0.0	0.0	0.0
53	0	0.971	-12.23	20.0	10.0	0.0	0.0	0.0	0.0
54	0	0.996	-11.69	4.1	1.4	0.0	0.0	0.0	0.0
55	0	1.031	-10.78	6.8	3.4	0.0	0.0	0.0	0.0
56	0	0.968	-16.04	7.6	2.2	0.0	0.0	0.0	0.0
57	0	0.965	-16.56	6.7	2.0	0.0	0.0	0.0	0.0

Table 13: IEEE 57 bus branch data

From	To	Rpu	Xpu	Tap
1	2	0,0083	0,028	0
2	3	0,0298	0,085	0
3	4	0,0112	0,0366	0
4	5	0,0625	0,132	0
4	6	0,043	0,148	0
6	7	0,02	0,102	0
6	8	0,0339	0,173	0
8	9	0,0099	0,0505	0
9	10	0,0369	0,1679	0
9	11	0,0258	0,0848	0
9	12	0,0648	0,295	0
9	13	0,0481	0,158	0
13	14	0,0132	0,0434	0
13	15	0,0269	0,0869	0
1	15	0,0178	0,091	0
1	16	0,0454	0,206	0
1	17	0,0238	0,108	0
3	15	0,0162	0,053	0
4	18	0	0,555	0,97
4	18	0	0,43	0,978
5	6	0,0302	0,0641	0
7	8	0,0139	0,0712	0
10	12	0,0277	0,1262	0
11	13	0,0223	0,0732	0
12	13	0,0178	0,058	0
12	16	0,018	0,0813	0
12	17	0,0397	0,179	0
14	15	0,0171	0,0547	0
18	19	0,461	0,685	0

From	To	Rpu	Xpu	Tap
19	20	0,283	0,434	0
21	20	0	0,7767	1,043
21	22	0,0736	0,117	0
22	23	0,0099	0,0152	0
23	24	0,166	0,256	0
24	25	0	1,182	1
24	25	0	1,23	1
24	26	0	0,0473	1,043
26	27	0,165	0,254	0
27	28	0,0618	0,0954	0
28	29	0,0418	0,0587	0
7	29	0	0,0648	0,967
25	30	0,135	0,202	0
30	31	0,326	0,497	0
31	32	0,507	0,755	0
32	33	0,0392	0,036	0
34	32	0	0,953	0,975
34	35	0,052	0,078	0
35	36	0,043	0,0537	0
36	37	0,029	0,0366	0
37	38	0,0651	0,1009	0
37	39	0,0239	0,0379	0
36	40	0,03	0,0466	0
22	38	0,0192	0,0295	0
11	41	0	0,749	0,955
41	42	0,207	0,352	0
41	43	0	0,412	0
38	44	0,0289	0,0585	0
15	45	0	0,1042	0,955
14	46	0	0,0735	0,9
46	47	0,023	0,068	0

From	To	Rpu	Xpu	Tap
47	48	0,0182	0,0233	0
48	49	0,0834	0,129	0
49	50	0,0801	0,128	0
50	51	0,1386	0,22	0
10	51	0	0,0712	0,93
13	49	0	0,191	0,895
29	52	0,1442	0,187	0
52	53	0,0762	0,0984	0
53	54	0,1878	0,232	0
54	55	0,1732	0,2265	0
11	43	0	0,153	0,958
44	45	0,0624	0,1242	0
40	56	0	1,195	0,958
56	41	0,553	0,549	0
56	42	0,2125	0,354	0
39	57	0	1,355	0,98
57	56	0,174	0,26	0
38	49	0,115	0,177	0
38	48	0,0312	0,0482	0
9	55	0	0,1205	0,94

A.4 IEEE 118 bus

Table 14: IEEE 118 bus data

N	Type	V	A	Pl	Ql	Pg	Qg	Qmax	Qmin
1	2	0.955	10.67	51.0	27.0	0.0	0.0	15.0	-5.0
2	0	0.971	11.22	20.0	9.0	0.0	0.0	0.0	0.0
3	0	0.968	11.56	39.0	10.0	0.0	0.0	0.0	0.0
4	2	0.998	15.28	30.0	12.0	-9.0	0.0	300.0	-300.0
5	0	1.002	15.73	0.0	0.0	0.0	0.0	0.0	0.0
6	2	0.990	13.00	52.0	22.0	0.0	0.0	50.0	-13.0
7	0	0.989	12.56	19.0	2.0	0.0	0.0	0.0	0.0
8	2	1.015	20.77	0.0	0.0	-28.0	0.0	300.0	-300.0
9	0	1.043	28.02	0.0	0.0	0.0	0.0	0.0	0.0
10	2	1.050	35.61	0.0	0.0	450.0	0.0	200.0	-147.0
11	0	0.985	12.72	70.0	23.0	0.0	0.0	0.0	0.0
12	2	0.990	12.20	47.0	10.0	85.0	0.0	120.0	-35.0
13	0	0.968	11.35	34.0	16.0	0.0	0.0	0.0	0.0
14	0	0.984	11.50	14.0	1.0	0.0	0.0	0.0	0.0
15	2	0.970	11.23	90.0	30.0	0.0	0.0	30.0	-10.0
16	0	0.984	11.91	25.0	10.0	0.0	0.0	0.0	0.0
17	0	0.995	13.74	11.0	3.0	0.0	0.0	0.0	0.0
18	2	0.973	11.53	60.0	34.0	0.0	0.0	50.0	-16.0
19	2	0.963	11.05	45.0	25.0	0.0	0.0	24.0	-8.0
20	0	0.958	11.93	18.0	3.0	0.0	0.0	0.0	0.0
21	0	0.959	13.52	14.0	8.0	0.0	0.0	0.0	0.0
22	0	0.970	16.08	10.0	5.0	0.0	0.0	0.0	0.0
23	0	1.000	21.00	7.0	3.0	0.0	0.0	0.0	0.0
24	2	0.992	20.89	0.0	0.0	-13.0	0.0	300.0	-300.0
25	2	1.050	27.93	0.0	0.0	220.0	0.0	140.0	-47.0
26	2	1.015	29.71	0.0	0.0	314.0	0.0	1000.0	-1000.0
27	2	0.968	15.35	62.0	13.0	-9.0	0.0	300.0	-300.0

N	Type	V	A	Pl	Ql	Pg	Qg	Qmax	Qmin
28	0	0.962	13.62	17.0	7.0	0.0	0.0	0.0	0.0
29	0	0.963	12.63	24.0	4.0	0.0	0.0	0.0	0.0
30	0	0.968	18.79	0.0	0.0	0.0	0.0	0.0	0.0
31	2	0.967	12.75	43.0	27.0	7.0	0.0	300.0	-300.0
32	2	0.964	14.80	59.0	23.0	0.0	0.0	42.0	-14.0
33	0	0.972	10.63	23.0	9.0	0.0	0.0	0.0	0.0
34	2	0.986	11.30	59.0	26.0	0.0	0.0	24.0	-8.0
35	0	0.981	10.87	33.0	9.0	0.0	0.0	0.0	0.0
36	2	0.980	10.87	31.0	17.0	0.0	0.0	24.0	-8.0
37	0	0.992	11.77	0.0	0.0	0.0	0.0	0.0	0.0
38	0	0.962	16.91	0.0	0.0	0.0	0.0	0.0	0.0
39	0	0.970	8.41	27.0	11.0	0.0	0.0	0.0	0.0
40	2	0.970	7.35	20.0	23.0	-46.0	0.0	300.0	-300.0
41	0	0.967	6.92	37.0	10.0	0.0	0.0	0.0	0.0
42	2	0.985	8.53	37.0	23.0	-59.0	0.0	300.0	-300.0
43	0	0.978	11.28	18.0	7.0	0.0	0.0	0.0	0.0
44	0	0.985	13.82	16.0	8.0	0.0	0.0	0.0	0.0
45	0	0.987	15.67	53.0	22.0	0.0	0.0	0.0	0.0
46	2	1.005	18.49	28.0	10.0	19.0	0.0	100.0	-100.0
47	0	1.017	20.73	34.0	0.0	0.0	0.0	0.0	0.0
48	0	1.021	19.93	20.0	11.0	0.0	0.0	0.0	0.0
49	2	1.025	20.94	87.0	30.0	204.0	0.0	210.0	-85.0
50	0	1.001	18.90	17.0	4.0	0.0	0.0	0.0	0.0
51	0	0.967	16.28	17.0	8.0	0.0	0.0	0.0	0.0
52	0	0.957	15.32	18.0	5.0	0.0	0.0	0.0	0.0
53	0	0.946	14.35	23.0	11.0	0.0	0.0	0.0	0.0
54	2	0.955	15.26	113.0	32.0	48.0	0.0	300.0	-300.0
55	2	0.952	14.97	63.0	22.0	0.0	0.0	23.0	-8.0
56	2	0.954	15.16	84.0	18.0	0.0	0.0	15.0	-8.0
57	0	0.971	16.36	12.0	3.0	0.0	0.0	0.0	0.0
58	0	0.959	15.51	12.0	3.0	0.0	0.0	0.0	0.0

N	Type	V	A	Pl	Ql	Pg	Qg	Qmax	Qmin
59	2	0.985	19.37	277.0	113.0	155.0	0.0	180.0	-60.0
60	0	0.993	23.15	78.0	3.0	0.0	0.0	0.0	0.0
61	2	0.995	24.04	0.0	0.0	160.0	0.0	300.0	-100.0
62	2	0.998	23.43	77.0	14.0	0.0	0.0	20.0	-20.0
63	0	0.969	22.75	0.0	0.0	0.0	0.0	0.0	0.0
64	0	0.984	24.52	0.0	0.0	0.0	0.0	0.0	0.0
65	2	1.005	27.65	0.0	0.0	391.0	0.0	200.0	-67.0
66	2	1.050	27.48	39.0	18.0	392.0	0.0	200.0	-67.0
67	0	1.020	24.84	28.0	7.0	0.0	0.0	0.0	0.0
68	0	1.003	27.55	0.0	0.0	0.0	0.0	0.0	0.0
69	3	1.035	30.00	0.0	0.0	516.4	0.0	300.0	-300.0
70	2	0.984	22.58	66.0	20.0	0.0	0.0	32.0	-10.0
71	0	0.987	22.15	0.0	0.0	0.0	0.0	0.0	0.0
72	2	0.980	20.98	0.0	0.0	-12.0	0.0	100.0	-100.0
73	2	0.991	21.94	0.0	0.0	-6.0	0.0	100.0	-100.0
74	2	0.958	21.64	68.0	27.0	0.0	0.0	9.0	-6.0
75	0	0.967	22.91	47.0	11.0	0.0	0.0	0.0	0.0
76	2	0.943	21.77	68.0	36.0	0.0	0.0	23.0	-8.0
77	2	1.006	26.72	61.0	28.0	0.0	0.0	70.0	-20.0
78	0	1.003	26.42	71.0	26.0	0.0	0.0	0.0	0.0
79	0	1.009	26.72	39.0	32.0	0.0	0.0	0.0	0.0
80	2	1.040	28.96	130.0	26.0	477.0	0.0	280.0	-165.0
81	0	0.997	28.10	0.0	0.0	0.0	0.0	0.0	0.0
82	0	0.989	27.24	54.0	27.0	0.0	0.0	0.0	0.0
83	0	0.985	28.42	20.0	10.0	0.0	0.0	0.0	0.0
84	0	0.980	30.95	11.0	7.0	0.0	0.0	0.0	0.0
85	2	0.985	32.51	24.0	15.0	0.0	0.0	23.0	-8.0
86	0	0.987	31.14	21.0	10.0	0.0	0.0	0.0	0.0
87	2	1.015	31.40	0.0	0.0	4.0	0.0	1000.0	-100.0
88	0	0.987	35.64	48.0	10.0	0.0	0.0	0.0	0.0
89	2	1.005	39.69	0.0	0.0	607.0	0.0	300.0	-210.0

N	Type	V	A	Pl	Ql	Pg	Qg	Qmax	Qmin
90	2	0.985	33.29	78.0	42.0	-85.0	0.0	300.0	-300.0
91	2	0.980	33.31	0.0	0.0	-10.0	0.0	100.0	-100.0
92	2	0.993	33.80	65.0	10.0	0.0	0.0	9.0	-3.0
93	0	0.987	30.79	12.0	7.0	0.0	0.0	0.0	0.0
94	0	0.991	28.64	30.0	16.0	0.0	0.0	0.0	0.0
95	0	0.981	27.67	42.0	31.0	0.0	0.0	0.0	0.0
96	0	0.993	27.51	38.0	15.0	0.0	0.0	0.0	0.0
97	0	1.011	27.88	15.0	9.0	0.0	0.0	0.0	0.0
98	0	1.024	27.40	34.0	8.0	0.0	0.0	0.0	0.0
99	2	1.010	27.04	0.0	0.0	-42.0	0.0	100.0	-100.0
100	2	1.017	28.03	37.0	18.0	252.0	0.0	155.0	-50.0
101	0	0.993	29.61	22.0	15.0	0.0	0.0	0.0	0.0
102	0	0.991	32.30	5.0	3.0	0.0	0.0	0.0	0.0
103	2	1.001	24.44	23.0	16.0	40.0	0.0	40.0	-15.0
104	2	0.971	21.69	38.0	25.0	0.0	0.0	23.0	-8.0
105	2	0.965	20.57	31.0	26.0	0.0	0.0	23.0	-8.0
106	0	0.962	20.32	43.0	16.0	0.0	0.0	0.0	0.0
107	2	0.952	17.53	28.0	12.0	-22.0	0.0	200.0	-200.0
108	0	0.967	19.38	2.0	1.0	0.0	0.0	0.0	0.0
109	0	0.967	18.93	8.0	3.0	0.0	0.0	0.0	0.0
110	2	0.973	18.09	39.0	30.0	0.0	0.0	23.0	-8.0
111	2	0.980	19.74	0.0	0.0	36.0	0.0	1000.0	-100.0
112	2	0.975	14.99	25.0	13.0	-43.0	0.0	1000.0	-100.0
113	2	0.993	13.74	0.0	0.0	-6.0	0.0	200.0	-100.0
114	0	0.960	14.46	8.0	3.0	0.0	0.0	0.0	0.0
115	0	0.960	14.46	22.0	7.0	0.0	0.0	0.0	0.0
116	2	1.005	27.12	0.0	0.0	-184.0	0.0	1000.0	-1000.0
117	0	0.974	10.67	20.0	8.0	0.0	0.0	0.0	0.0
118	0	0.949	21.92	33.0	15.0	0.0	0.0	0.0	0.0

Table 15: IEEE 118 bus branch data

From	To	Rpu	Xpu	Tap
1	2	0.03030	0.09990	0.0
1	3	0.01290	0.04240	0.0
4	5	0.00176	0.00798	0.0
3	5	0.02410	0.10800	0.0
5	6	0.01190	0.05400	0.0
6	7	0.00459	0.02080	0.0
8	9	0.00244	0.03050	0.0
8	5	0.00000	0.02670	0.985
9	10	0.00258	0.03220	0.0
4	11	0.02090	0.06880	0.0
5	11	0.02030	0.06820	0.0
11	12	0.00595	0.01960	0.0
2	12	0.01870	0.06160	0.0
3	12	0.04840	0.16000	0.0
7	12	0.00862	0.03400	0.0
11	13	0.02225	0.07310	0.0
12	14	0.02150	0.07070	0.0
13	15	0.07440	0.24440	0.0
14	15	0.05950	0.19500	0.0
12	16	0.02120	0.08340	0.0
15	17	0.01320	0.04370	0.0
16	17	0.04540	0.18010	0.0
17	18	0.01230	0.05050	0.0
18	19	0.01119	0.04930	0.0
19	20	0.02520	0.11700	0.0
15	19	0.01200	0.03940	0.0
20	21	0.01830	0.08490	0.0
21	22	0.02090	0.09700	0.0
22	23	0.03420	0.15900	0.0

From	To	Rpu	Xpu	Tap
23	24	0.01350	0.04920	0.0
23	25	0.01560	0.08000	0.0
26	25	0.00000	0.03820	0.960
25	27	0.03180	0.16300	0.0
27	28	0.01913	0.08550	0.0
28	29	0.02370	0.09430	0.0
30	17	0.00000	0.03880	0.960
8	30	0.00431	0.05040	0.0
26	30	0.00799	0.08600	0.0
17	31	0.04740	0.15630	0.0
29	31	0.01080	0.03310	0.0
23	32	0.03170	0.11530	0.0
31	32	0.02980	0.09850	0.0
27	32	0.02290	0.07550	0.0
15	33	0.03800	0.12440	0.0
19	34	0.07520	0.24700	0.0
35	36	0.00224	0.01020	0.0
35	37	0.01100	0.04970	0.0
33	37	0.04150	0.14200	0.0
34	36	0.00871	0.02680	0.0
34	37	0.00256	0.00940	0.0
38	37	0.00000	0.03750	0.935
37	39	0.03210	0.10600	0.0
37	40	0.05930	0.16800	0.0
30	38	0.00464	0.05400	0.0
39	40	0.01840	0.06050	0.0
40	41	0.01450	0.04870	0.0
40	42	0.05550	0.18300	0.0
41	42	0.04100	0.13500	0.0
43	44	0.06080	0.24540	0.0
34	43	0.04130	0.16810	0.0

From	To	Rpu	Xpu	Tap
44	45	0.02240	0.09010	0.0
45	46	0.04000	0.13560	0.0
46	47	0.03800	0.12700	0.0
46	48	0.06010	0.18900	0.0
47	49	0.01910	0.06250	0.0
42	49	0.07150	0.32300	0.0
42	49	0.07150	0.32300	0.0
45	49	0.06840	0.18600	0.0
48	49	0.01790	0.05050	0.0
49	50	0.02670	0.07520	0.0
49	51	0.04860	0.13700	0.0
51	52	0.02030	0.05880	0.0
52	53	0.04050	0.16350	0.0
53	54	0.02630	0.12200	0.0
49	54	0.07300	0.28900	0.0
49	54	0.08690	0.29100	0.0
54	55	0.01690	0.07070	0.0
54	56	0.00275	0.00955	0.0
55	56	0.00488	0.01510	0.0
56	57	0.03430	0.09660	0.0
50	57	0.04740	0.13400	0.0
56	58	0.03430	0.09660	0.0
51	58	0.02550	0.07190	0.0
54	59	0.05030	0.22930	0.0
56	59	0.08250	0.25100	0.0
56	59	0.08030	0.23900	0.0
55	59	0.04739	0.21580	0.0
59	60	0.03170	0.14500	0.0
59	61	0.03280	0.15000	0.0
60	61	0.00264	0.01350	0.0
60	62	0.01230	0.05610	0.0

From	To	Rpu	Xpu	Tap
61	62	0.00824	0.03760	0.0
63	59	0.00000	0.03860	0.960
63	64	0.00172	0.02000	0.0
64	61	0.00000	0.02680	0.985
38	65	0.00901	0.09860	0.0
64	65	0.00269	0.03020	0.0
49	66	0.01800	0.09190	0.0
49	66	0.01800	0.09190	0.0
62	66	0.04820	0.21800	0.0
62	67	0.02580	0.11700	0.0
65	66	0.00000	0.03700	0.935
66	67	0.02240	0.10150	0.0
65	68	0.00138	0.01600	0.0
47	69	0.08440	0.27780	0.0
49	69	0.09850	0.32400	0.0
68	69	0.00000	0.03700	0.935
69	70	0.03000	0.12700	0.0
24	70	0.00221	0.41150	0.0
70	71	0.00882	0.03550	0.0
24	72	0.04880	0.19600	0.0
71	72	0.04460	0.18000	0.0
71	73	0.00866	0.04540	0.0
70	74	0.04010	0.13230	0.0
70	75	0.04280	0.14100	0.0
69	75	0.04050	0.12200	0.0
74	75	0.01230	0.04060	0.0
76	77	0.04440	0.14800	0.0
69	77	0.03090	0.10100	0.0
75	77	0.06010	0.19990	0.0
77	78	0.00376	0.01240	0.0
78	79	0.00546	0.02440	0.0

From	To	Rpu	Xpu	Tap
77	80	0.01700	0.04850	0.0
77	80	0.02940	0.10500	0.0
79	80	0.01560	0.07040	0.0
68	81	0.00175	0.02020	0.0
81	80	0.00000	0.03700	0.935
77	82	0.02980	0.08530	0.0
82	83	0.01120	0.03665	0.0
83	84	0.06250	0.13200	0.0
83	85	0.04300	0.14800	0.0
84	85	0.03020	0.06410	0.0
85	86	0.03500	0.12300	0.0
86	87	0.02828	0.20740	0.0
85	88	0.02000	0.10200	0.0
85	89	0.02390	0.17300	0.0
88	89	0.01390	0.07120	0.0
89	90	0.05180	0.18800	0.0
89	90	0.02380	0.09970	0.0
90	91	0.02540	0.08360	0.0
89	92	0.00990	0.05050	0.0
89	92	0.03930	0.15810	0.0
91	92	0.03870	0.12720	0.0
92	93	0.02580	0.08480	0.0
92	94	0.04810	0.15800	0.0
93	94	0.02230	0.07320	0.0
94	95	0.01320	0.04340	0.0
80	96	0.03560	0.18200	0.0
82	96	0.01620	0.05300	0.0
94	96	0.02690	0.08690	0.0
80	97	0.01830	0.09340	0.0
80	98	0.02380	0.10800	0.0
80	99	0.04540	0.20600	0.0

From	To	Rpu	Xpu	Tap
92	100	0.06480	0.29500	0.0
94	100	0.01780	0.05800	0.0
95	96	0.01710	0.05470	0.0
96	97	0.01730	0.08850	0.0
98	100	0.03970	0.17900	0.0
99	100	0.01800	0.08130	0.0
100	101	0.02770	0.12620	0.0
92	102	0.01230	0.05590	0.0
101	102	0.02460	0.11200	0.0
100	103	0.01600	0.05250	0.0
100	104	0.04510	0.20400	0.0
103	104	0.04660	0.15840	0.0
103	105	0.05350	0.16250	0.0
100	106	0.06050	0.22900	0.0
104	105	0.00994	0.03780	0.0
105	106	0.01400	0.05470	0.0
105	107	0.05300	0.18300	0.0
105	108	0.02610	0.07030	0.0
106	107	0.05300	0.18300	0.0
108	109	0.01050	0.02880	0.0
103	110	0.03906	0.18130	0.0
109	110	0.02780	0.07620	0.0
110	111	0.02200	0.07550	0.0
110	112	0.02470	0.06400	0.0
17	113	0.00913	0.03010	0.0
32	113	0.06150	0.20300	0.0
32	114	0.01350	0.06120	0.0
27	115	0.01640	0.07410	0.0
114	115	0.00230	0.01040	0.0
68	116	0.00034	0.00405	0.0
12	117	0.03290	0.14000	0.0

From	To	Rpu	Xpu	Tap
75	118	0.01450	0.04810	0.0
76	118	0.01640	0.05440	0.0

A.5 Brazilian 107 Bus test system

Table 16: System data - Brazilian 107 Bus test system

N	Type	V	A	Pl	Ql	Pg	Qg	Qmax	Qmin
12	1	1.000	-24.0	110.0	0.0	300.0	-203.0	420.0	-540.0
16	1	1.000	-26.0	110.0	0.0	800.0	-134.0	480.0	-720.0
18	2	1.020	-24.0	110.0	0.0	995.7	-401.0	600.0	-546.0
20	1	1.010	-22.0	110.0	0.0	900.0	-321.0	640.0	-640.0
21	1	1.000	-62.0	310.0	0.0	160.0	-25.8	84.0	-80.0
22	1	1.000	-20.0	110.0	0.0	150.0	-20.6	126.0	-120.0
35	1	1.000	-27.0	110.0	0.0	200.0	-50.0	180.0	-180.0
48	1	1.000	-43.0	110.0	0.0	0.0	-461.0	1200.0	-1080.0
86	0	1.033	-43.0	110.0	66.0	0.0	0.0	0.0	0.0
100	0	1.056	-28.0	110.0	0.0	0.0	0.0	0.0	0.0
101	0	1.069	-36.0	110.0	0.0	0.0	0.0	0.0	-200.0
102	0	1.059	-43.0	110.0	0.0	0.0	0.0	0.0	-100.0
103	0	1.072	-43.0	110.0	0.0	0.0	0.0	0.0	0.0
104	0	1.061	-52.0	110.0	910.0	0.0	0.0	0.0	235.0
106	0	1.050	-53.0	110.0	0.0	0.0	0.0	0.0	-100.0
120	0	1.041	-41.0	110.0	180.0	0.0	0.0	0.0	90.0
122	0	1.067	-42.0	110.0	200.0	0.0	0.0	0.0	38.0
123	0	1.035	-46.0	110.0	450.0	0.0	0.0	0.0	175.0
126	0	1.037	-43.0	110.0	290.0	0.0	0.0	0.0	95.0
131	0	1.027	-27.0	110.0	0.0	0.0	0.0	0.0	0.0
134	0	1.027	-26.0	110.0	0.0	0.0	0.0	0.0	0.0
136	0	1.028	-33.0	110.0	54.0	0.0	0.0	0.0	23.0

N	Type	V	A	Pl	Ql	Pg	Qg	Qmax	Qmin
138	0	1.036	-44.0	110.0	72.0	0.0	0.0	0.0	34.0
140	0	1.023	-54.0	110.0	700.0	0.0	0.0	0.0	250.0
210	0	1.048	-28.0	110.0	0.0	0.0	0.0	0.0	0.0
213	0	1.050	-29.0	110.0	93.0	0.0	0.0	0.0	39.0
216	0	1.049	-28.0	110.0	53.0	0.0	0.0	0.0	25.0
217	0	1.050	-32.0	110.0	364.0	0.0	0.0	0.0	58.0
218	0	1.025	-40.0	110.0	600.0	0.0	0.0	0.0	200.0
219	0	1.028	-39.0	110.0	0.0	0.0	0.0	0.0	0.0
220	0	1.052	-32.0	110.0	0.0	0.0	0.0	0.0	0.0
225	0	1.000	-35.0	110.0	0.0	0.0	0.0	0.0	0.0
228	0	1.016	-41.0	110.0	86.0	0.0	0.0	0.0	34.0
231	0	1.013	-49.0	310.0	89.7	0.0	0.0	0.0	31.9
233	0	1.039	-36.0	110.0	0.0	0.0	0.0	0.0	0.0
234	0	1.027	-39.0	110.0	1000.0	0.0	0.0	0.0	350.0
300	1	1.020	-19.0	110.0	0.0	700.0	-184.0	392.0	-440.0
301	1	1.010	-19.0	110.0	0.0	300.0	-129.0	140.0	-140.0
302	1	1.020	-18.0	110.0	0.0	400.0	-125.0	150.0	-150.0
303	1	1.020	-24.0	110.0	0.0	200.0	-279.0	600.0	-600.0
305	1	1.000	-22.0	110.0	0.0	300.0	-60.5	120.0	-120.0
320	0	1.049	-24.0	110.0	0.0	0.0	0.0	0.0	0.0
325	0	1.046	-24.0	110.0	0.0	0.0	0.0	0.0	0.0
326	0	1.033	-26.0	110.0	274.0	0.0	0.0	0.0	104.0
360	0	1.047	-22.0	110.0	0.0	0.0	0.0	0.0	0.0
370	0	1.049	-25.0	110.0	0.0	0.0	0.0	0.0	0.0
396	0	1.041	-26.0	110.0	0.0	0.0	0.0	0.0	0.0
500	1	1.020	-22.0	110.0	0.0	800.0	-118.0	540.0	-540.0
535	0	1.035	-26.0	110.0	0.0	0.0	0.0	0.0	0.0
536	0	1.023	-29.0	110.0	700.0	0.0	0.0	0.0	150.0
800	1	1.020	-7.0	210.0	0.0	1100.0	138.8	800.0	-800.0
808	1	1.020	3.5	210.0	0.0	1150.0	113.3	600.0	-600.0
810	1	1.020	-4.0	210.0	0.0	1200.0	-72.0	532.0	-400.0

N	Type	V	A	Pl	Ql	Pg	Qg	Qmax	Qmin
814	0	1.000	-38.0	210.0	735.4	0.0	0.0	0.0	191.0
824	0	1.038	-17.0	210.0	0.0	0.0	0.0	0.0	0.0
834	0	0.994	-29.0	210.0	13.4	0.0	0.0	0.0	4.2
839	0	0.999	-6.4	210.0	0.0	0.0	0.0	0.0	0.0
840	0	0.986	-9.4	210.0	159.0	0.0	0.0	0.0	36.0
848	0	0.999	-5.5	210.0	94.0	0.0	0.0	0.0	18.0
856	0	1.035	-11.0	210.0	0.0	0.0	0.0	0.0	0.0
895	0	1.044	-35.0	210.0	0.0	0.0	0.0	0.0	0.0
896	0	1.028	-4.3	210.0	0.0	0.0	0.0	0.0	0.0
897	0	1.040	-3.0	210.0	0.0	0.0	0.0	0.0	0.0
898	0	1.012	-2.1	210.0	0.0	0.0	0.0	0.0	0.0
904	1	1.020	-15.0	210.0	0.0	700.0	-236.0	475.0	-475.0
915	1	1.020	-13.0	210.0	0.0	700.0	-109.0	465.0	-516.0
919	1	1.000	5.75	210.0	0.0	700.0	88.63	220.0	-148.0
925	1	1.020	-0.12	210.0	0.0	950.0	72.93	420.0	-440.0
933	0	1.038	-18.0	210.0	0.0	0.0	0.0	0.0	0.0
934	0	1.000	-18.0	210.0	237.0	0.0	0.0	0.0	59.0
938	0	1.043	-37.0	210.0	0.0	0.0	0.0	0.0	0.0
939	0	1.000	-40.0	210.0	1149.0	0.0	0.0	0.0	53.06
955	0	1.058	-24.0	210.0	0.0	0.0	0.0	0.0	0.0
959	0	1.033	-35.0	210.0	0.0	0.0	0.0	0.0	100.0
960	0	1.000	-38.0	210.0	844.74	0.0	0.0	0.0	469.1
964	0	1.037	-31.0	210.0	0.0	0.0	0.0	0.0	0.0
965	0	1.000	-33.0	210.0	755.6	0.0	0.0	0.0	56.24
976	0	1.012	-34.0	210.0	0.0	0.0	0.0	0.0	0.0
995	0	1.050	-19.0	210.0	0.0	0.0	0.0	0.0	0.0
1015	0	1.002	-40.0	210.0	70.0	0.0	0.0	0.0	2.0
1030	0	1.052	-21.0	210.0	0.0	0.0	0.0	0.0	0.0
1047	0	1.017	-1.2	210.0	0.0	0.0	0.0	0.0	0.0
1060	0	1.043	-8.1	210.0	0.0	0.0	0.0	0.0	0.0
1210	0	1.000	-36.0	210.0	1228.0	0.0	0.0	0.0	425.0

N	Type	V	A	Pl	Ql	Pg	Qg	Qmax	Qmin
1503	0	1.061	-50.0	110.0	0.0	0.0	0.0	0.0	0.0
1504	0	1.026	-53.0	110.0	145.0	0.0	0.0	0.0	63.0
2458	0	1.000	-6.6	210.0	403.0	0.0	0.0	0.0	126.0
4501	0	1.030	-61.0	310.0	31.4	0.0	0.0	0.0	7.1
4521	0	1.037	-66.0	310.0	0.0	0.0	0.0	0.0	0.0
4522	0	1.037	-68.0	310.0	0.0	0.0	0.0	0.0	-20.0
4523	1	1.010	-61.0	310.0	0.0	50.0	-10.8	30.0	-42.0
4530	0	1.048	-73.0	310.0	0.0	0.0	0.0	0.0	0.0
4532	0	1.048	-73.0	310.0	0.0	0.0	0.0	0.0	0.0
4533	0	1.018	-73.0	310.0	75.4	0.0	0.0	0.0	16.1
4542	0	1.030	-72.0	310.0	0.0	0.0	0.0	0.0	0.0
4552	0	1.013	-80.0	410.0	12.6	0.0	0.0	0.0	1.2
4562	0	1.019	-88.0	410.0	23.8	0.0	0.0	0.0	7.4
4572	0	1.016	-85.0	410.0	18.0	0.0	0.0	0.0	6.4
4582	0	1.026	-91.0	410.0	85.5	0.0	0.0	0.0	21.8
4592	0	1.020	-67.0	310.0	0.0	0.0	0.0	0.0	0.0
4596	1	1.000	-68.0	310.0	0.0	230.0	-39.0	160.0	-160.0
4623	0	1.023	-71.0	310.0	128.24	0.0	0.0	0.0	40.76
4703	0	1.007	-74.0	310.0	182.0	0.0	0.0	0.0	129.75
4804	1	1.000	-75.0	310.0	0.0	50.0	-19.0	59.0	-86.0
4805	0	1.028	-78.0	310.0	0.0	0.0	0.0	0.0	0.0
4807	0	1.028	-80.0	310.0	128.9	0.0	0.0	0.0	36.3
4862	0	1.051	-78.0	310.0	0.0	0.0	0.0	0.0	-30.0

Table 17: Branch data - Brazilian 107 Bus test system

De	Para	Rpu	Xpu	Tap
86	48	0.00000	0.71475	1.000
86	122	0.00000	1.91300	1.000
86	122	0.00000	1.91300	1.000
100	20	0.00000	1.26400	1.000
100	101	0.17200	2.72000	1.000
100	101	0.17100	2.70000	1.000
100	210	0.20900	2.93500	1.000
100	213	0.00000	2.35700	1.000
100	535	0.15300	2.40000	1.000
101	102	0.15600	2.46000	1.000
101	103	0.15200	2.39000	1.000
102	120	0.00000	2.40300	1.000
102	1503	0.11000	1.91100	1.000
103	123	0.00000	2.41900	1.000
104	103	0.19600	3.10000	1.000
104	1503	0.05000	0.82000	1.000
106	104	0.15200	2.39000	1.000
106	104	0.15200	2.39000	1.000
106	140	0.00000	2.92300	1.000
106	140	0.00000	2.66800	1.000
122	103	0.10500	1.61900	1.000
123	120	0.35900	3.94500	1.000
126	86	0.10900	1.82600	1.000
126	86	0.10900	1.82400	1.000
126	120	0.60000	5.95000	1.000
126	120	0.60600	6.02000	1.000
131	22	0.00000	8.83330	1.000
134	12	0.00000	1.33500	0.999

From	To	Rpu	Xpu	Tap
134	131	0.09200	1.01000	1.000
134	396	0.32000	3.50900	1.000
136	16	0.00000	1.53600	1.000
136	120	0.43600	4.30000	1.000
136	120	0.43600	4.30000	1.000
136	131	0.34800	3.42000	1.000
136	134	0.37500	4.13000	1.000
136	138	0.64900	6.46000	1.000
136	138	0.55800	6.19000	1.000
140	138	0.65200	6.50000	1.000
140	138	0.55800	6.19000	1.000
210	18	0.00000	0.66667	1.000
210	217	0.00000	1.72000	1.000
210	217	0.00000	1.72000	1.000
210	370	0.14700	2.32000	1.000
213	216	0.21900	2.42000	1.000
216	396	0.12900	1.41400	1.000
217	216	0.56500	6.24800	1.000
217	218	0.50700	5.61000	1.000
217	218	0.50700	5.61000	1.000
218	234	0.43000	4.79900	1.000
218	234	0.43000	4.79900	1.000
219	234	0.03500	0.43300	1.000
219	234	0.03500	0.43300	1.000
220	35	0.00000	4.49650	1.025
220	217	0.22600	2.39600	1.000
220	219	0.72600	7.70400	1.000
225	217	0.00000	2.72100	0.955
225	217	0.00000	2.93800	0.955
225	231	4.10000	19.76000	1.000
225	231	1.27000	13.62000	1.000

From	To	Rpu	Xpu	Tap
228	219	0.00000	3.59500	1.000
231	4501	4.51000	21.69000	1.000
231	4501	1.49000	16.09000	1.000
233	210	0.28000	3.99300	1.000
233	320	0.27000	3.87300	1.000
234	233	0.00000	1.11300	1.000
234	233	0.00000	1.00000	1.000
320	210	0.12500	1.93700	1.000
320	300	0.00000	1.35670	1.000
320	360	0.08200	1.25600	1.000
325	301	0.00000	2.63250	1.000
325	326	0.00000	2.16000	1.000
325	326	0.00000	2.16000	1.000
325	360	0.10000	1.51900	1.000
325	370	0.28000	4.84000	1.000
326	134	0.07000	0.76100	1.000
326	396	0.24000	2.74000	1.000
360	302	0.00000	1.93670	1.000
370	303	0.00000	1.05750	1.000
370	535	0.09311	1.37580	1.000
396	305	0.00000	2.20000	1.025
535	500	0.00000	1.02500	1.000
536	535	0.00000	1.53300	1.000
536	535	0.00000	1.42000	1.000
814	895	0.03200	1.14600	0.9695
814	895	0.03100	1.16510	0.9695
824	800	0.00000	1.68000	1.024
824	933	0.01000	0.12400	1.000
824	933	0.01000	0.12600	1.000
834	934	2.44400	12.65200	1.000
839	840	0.00000	6.64000	1.000

From	To	Rpu	Xpu	Tap
839	840	0.00000	6.29000	1.000
839	898	1.13000	6.99000	1.000
839	1047	1.22000	7.69000	1.000
839	2458	0.22000	1.09000	1.000
839	2458	0.17000	1.03200	1.000
856	810	0.00000	1.05000	1.000
856	933	0.05200	0.65400	1.000
856	1060	0.05600	0.69700	1.000
895	122	0.30800	3.95800	1.000
895	122	0.30800	3.95800	1.000
896	897	0.05000	0.73000	1.000
897	808	0.00000	1.02000	1.024
898	848	0.00000	6.36000	1.000
898	1047	0.15000	0.89100	1.000
933	895	0.20000	2.55300	1.000
933	955	0.16200	2.04800	1.000
933	959	0.20000	2.69000	1.000
934	933	0.03100	1.20700	0.9766
934	1047	3.04500	15.73800	1.000
934	1047	3.04100	15.71800	1.000
938	955	0.25562	2.92240	1.000
938	959	0.12700	1.60300	1.000
939	938	0.03100	1.15000	0.9621
939	938	0.03200	1.16300	0.9621
939	938	0.00000	1.27700	0.9621
939	1015	1.27100	6.56200	1.000
939	1015	1.28300	6.56400	1.000
955	964	0.18772	2.34670	1.000
959	895	0.05000	0.44000	1.000
960	834	2.21000	11.47500	1.000
960	959	0.03200	1.16300	0.9961

From	To	Rpu	Xpu	Tap
960	959	0.03100	1.16600	0.9961
960	1015	1.89200	9.77600	1.000
960	1015	1.89500	9.70400	1.000
964	976	0.07330	0.91640	1.000
965	964	0.02000	1.21100	0.9687
965	964	0.02000	1.23300	0.9687
976	995	0.28200	3.85200	1.000
995	904	0.00000	1.15380	1.000
995	964	0.16433	3.03390	1.000
995	1030	0.07300	0.92100	1.000
995	1060	0.17200	2.17200	1.000
1030	915	0.00000	2.06550	1.000
1030	955	0.04700	0.59700	1.000
1047	919	0.00000	1.70220	1.025
1060	897	0.07600	1.17100	1.000
1060	925	0.00000	1.51500	1.024
1210	976	0.03000	1.21900	1.007
1210	976	0.03900	1.13800	1.007
1210	976	0.03600	1.21700	1.007
1503	1504	0.00000	5.20000	1.000
2458	896	0.00000	1.27000	0.9927
4501	4522	3.76000	20.68000	1.000
4501	4522	1.64000	12.46000	1.000
4521	4523	0.00000	20.71000	1.000
4522	4521	1.53000	7.60000	1.000
4522	4532	3.25000	17.92000	1.000
4522	4532	3.25000	17.92000	1.000
4522	4623	0.00000	7.95000	1.000
4522	4623	0.00000	7.95000	1.000
4532	4530	0.00000	14.30000	1.000
4532	4533	0.00000	8.60000	1.000

From	To	Rpu	Xpu	Tap
4532	4533	0.00000	8.60000	1.000
4532	4533	0.00000	8.60000	1.000
4532	4542	1.62000	9.68000	1.000
4533	4596	0.00000	3.76350	1.000
4542	4552	1.83000	10.93000	1.000
4552	4572	1.40000	8.38000	1.000
4562	4572	0.94000	5.59000	1.000
4562	4582	1.24000	7.38000	1.000
4592	21	0.00000	6.40000	1.000
4592	4542	1.00000	6.17000	1.000
4623	4533	17.06000	45.50000	1.000
4703	4533	0.90000	2.31000	1.000
4703	4533	0.90000	2.31000	1.000
4805	4804	0.00000	13.33300	1.000
4805	4807	3.08900	8.13400	1.000
4805	4807	3.08900	8.13400	1.000
4862	4532	2.57000	23.68000	1.000
4862	4532	2.57000	23.68000	1.000
4862	4807	0.00000	4.05000	1.000